

## 6

---

# STRUCTURE

---

### INTRODUCTION

Almost all plated metals are crystalline, which means that the atoms are arranged on a regular three dimensional pattern called a lattice (1). The three most important lattices are face centered cubic (fcc), body centered cubic (bcc) and hexagonal close packed (hcp), all shown in Figure 1. Face centered cubic packing of spheres often seen in fruit stands or in piles of cannonballs at war memorials, is the densest packing of spheres in three dimensional space (2,3,4). Table 1 lists the lattices for the commonly plated metals. However, it's important to note that incorporation of foreign species can modify the structure of deposited metals. For example, a structural transition from unstable hexagonal chromium hydride to body centered cubic chromium during or soon after plating accounts for the cracking observed in chromium deposits. This decomposition involves a volume shrinkage of greater than 15 percent (5). More discussion on microstructural transformations of deposits will be presented later in this chapter. Additional topics that will be covered include texture and fractals.

### STRUCTURE OF ELECTRODEPOSITED AND ELECTROLESS COATINGS

The properties of all materials are determined by their structure. Even minor structural differences often have profound effects on the properties of electrodeposited metals (6). Four typical structures encountered with electrodeposited metals include; 1) columnar, 2) fibrous, 3) fine-grained, and 4) banded (7). Cross sections showing each type are

**Table 1 - Lattice Structure of Commonly Plated Metals**

Face centered cubic	Hexagonal close pack	Body centered cubic	Tetragonal
Ag Al Au Cu Ni Pb Pd Pt Rh	Cd Co Zn	Cr Fe	Sn

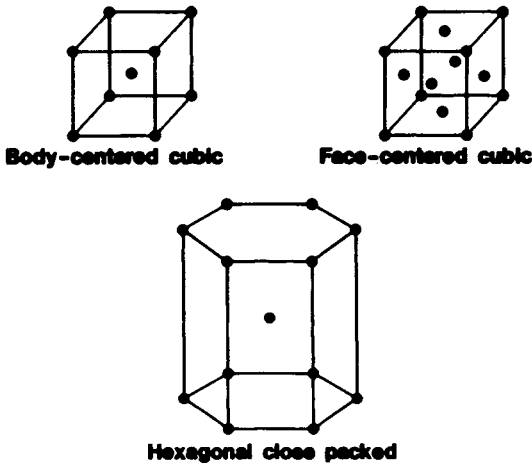


**Figure 1: Unit cells of the three most important lattices.**

included in Figures 2 to 6.

Columnar structures (Figure 2) are characteristic of deposits from simple ion acidic solutions containing no addition agents, e.g., copper, zinc, or tin from sulfate or fluoborate solutions, operated at elevated temperature or low current density. Deposits of this type usually exhibit lower strength and hardness than other structures but high ductility.

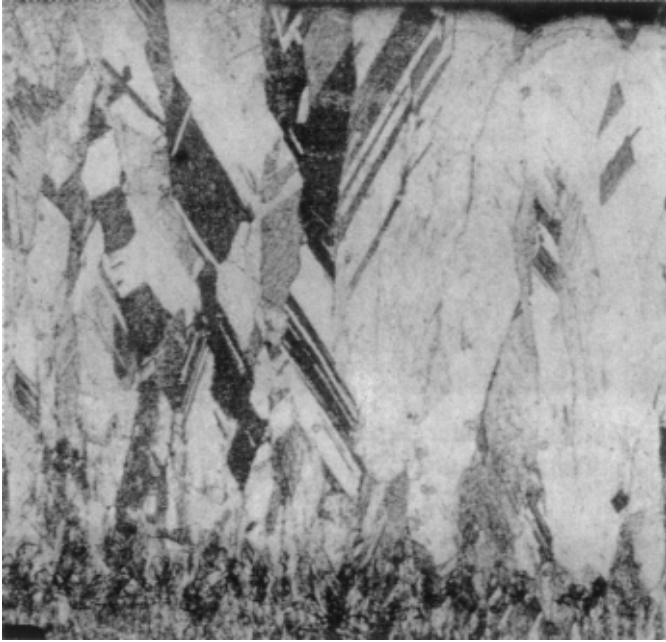


**Figure 2:** Large, Columnar Grains-cross section of a deposit produced in a citrate based acid gold solution (200 ×).

Fibrous (acicular) structures, which represent a refinement of columnar structure, are shown in Figure 3. This type of structure is obtained because some factors in the deposition process such as the presence of addition agents, or use of low temperature and high current density in copper sulfate solutions, have favored the formation of new nuclei rather than growth of existing grains. The finer grain size may be the result of interference of crystal growth by codeposited metal hydroxide or hydrogen (7). Properties of fibrous deposits are intermediate between columnar and fine-grained deposits.

Fine-grained structures (Figure 4) are usually obtained from complex ion solutions such as cyanide or with certain addition agents. These deposits are less pure, less dense and exhibit higher electrical resistivities due to the presence of codeposited foreign material. Deposits from simple ion acidic solutions, such as copper or nickel from sulfate solutions, develop this structure if operating conditions are more extreme

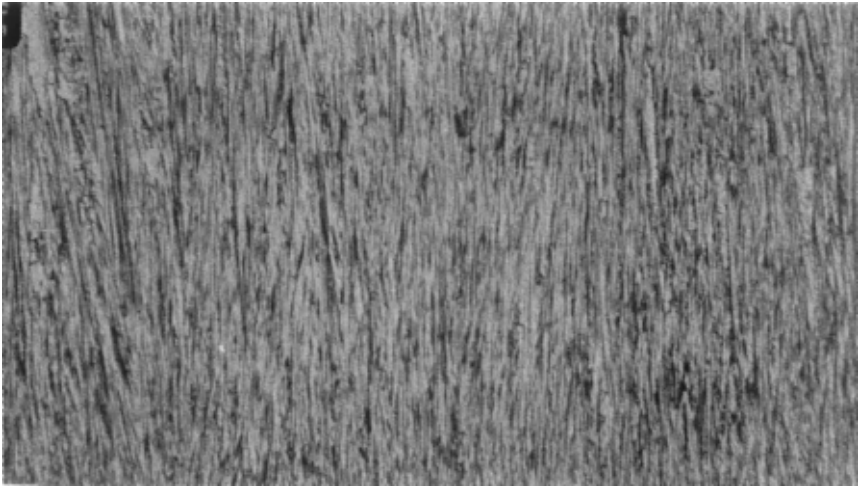


**Figure 3:** Fibrous (Acicular) Structure—cross section of a deposit produced in a nickel sulfamate solution (200  $\times$ ).

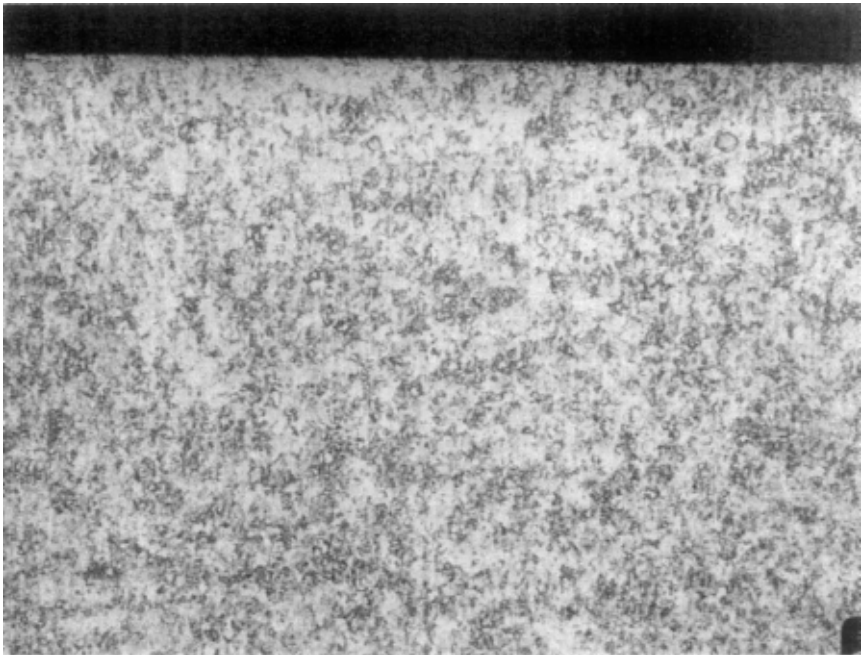


**Figure 4:** Fine Grained Structure—cross section of a deposit produced in a copper cyanide solution (200  $\times$ ).

than those that produce deposits of the type shown in Figure 3. For example, a very high current density, a high pH (in the case of a nickel solution) resulting in codeposited hydrated oxides, or certain addition agents may cause the formation of this type of structure (7). The grain sizes in deposits of this type are of the order of  $10^{-5}$  to  $10^{-6}$  cm. These deposits are usually relatively hard, strong and brittle but it is important to realize that some fine-grained structures can be quite ductile (30% elongation) and the grain size so small that it is virtually unresolvable, as shown in Figure 5 (8).

Laminar (or banded) structures are shown in Figure 6. The grains within the lamellae are extremely small. These structures are characteristic of bright deposits resulting from addition agents such as sulfur containing organic compounds which result in small amounts of S and C in the deposit. A number of alloy deposits such as gold-copper, cobalt-phosphorus, cobalt-tungsten, and nickel-phosphorus (electroless and electrodeposited) exhibit this structure. These deposits usually have high strength and hardness but low ductility. Similar laminations can be found in deposits produced in solutions operated with either periodic reverse current or pulse plating.

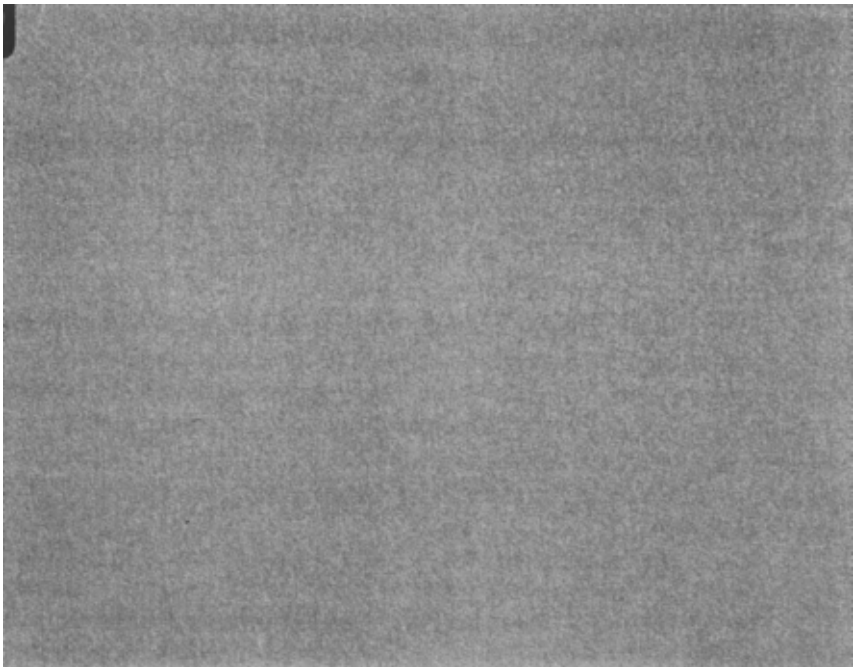


**Figure 5:** Very Fine Grained Structure—cross section of a deposit produced in a copper sulfate solution containing proprietary additives (500  $\times$ ).

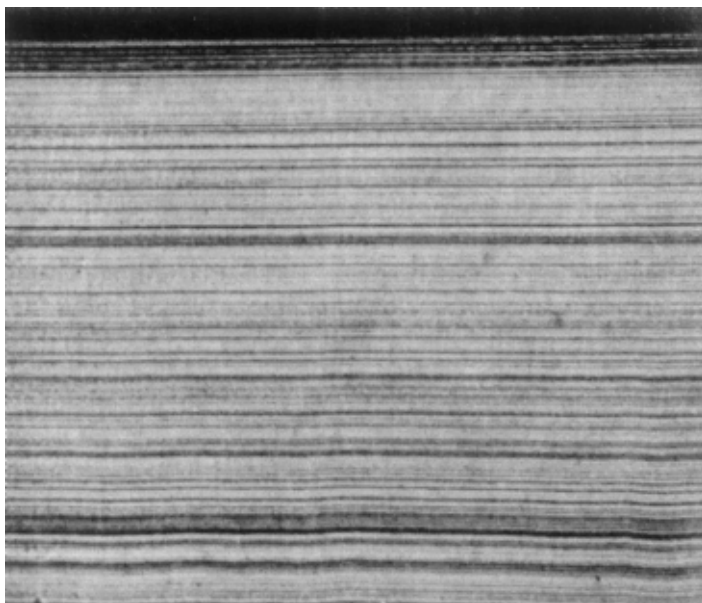


**Figure 6:** Laminated (or Banded) Structure—cross section of a gold-copper deposit (250  $\times$ ).

The crystal structure resulting from an electrodeposition process is strongly dependent on the relative rates of formation of crystal nuclei and the growth of existing crystals (9,10). Finer-grained deposits are the result of conditions that favor crystal nuclei formation while larger crystals are obtained in those cases that favor growth of existing crystals. Generally, a decreasing crystal size is the result of factors which increase the cathode polarization (9,10).

From the electroplaters' viewpoint, it would be nice to have some three dimensional picture that would show the influence of operating conditions on structure. However, since plating processes have numerous variables that influence structure, e.g., metal ion concentration, addition agents, current density, temperature, agitation, and polarization, a plot such as that shown in Figures 8 and 9 for physically vapor deposited films cannot be produced. However, Figure 7 does pictorially show how individual plating variables influence grain size of electrodeposits (11).

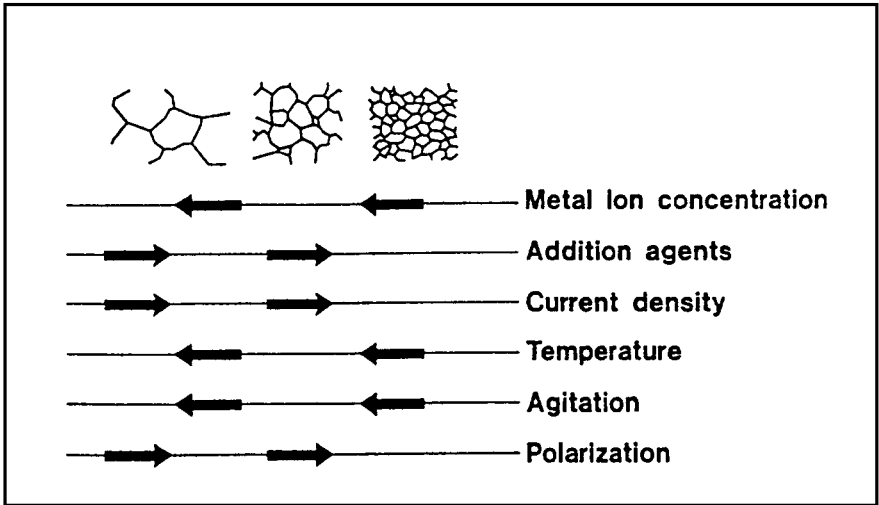


**Figure 7:** Relation of structure of electrodeposits to operating conditions of solutions. From reference 11.

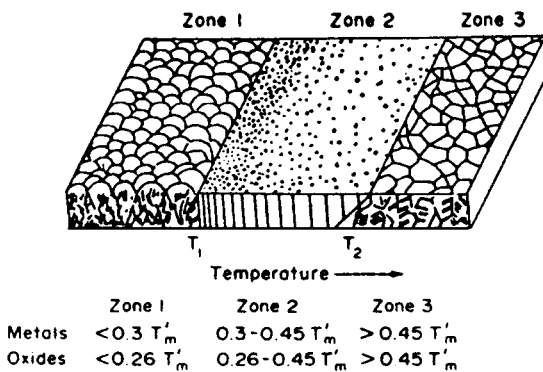


**Figure 8:** Structural zones in PVD films. From Movchan and Demchishin, reference 13. Reprinted with permission of Noyes Publications.

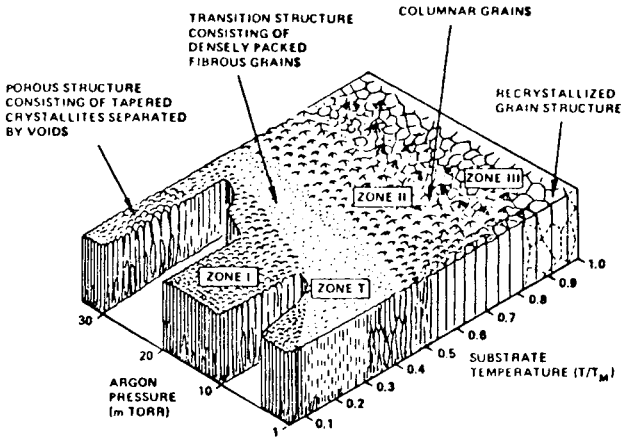


**Figure 9:** Structural zones in PVD films. From Thornton, references 14, 15. Reprinted with permission of Noyes Publications.

## STRUCTURE OF PHYSICALLY VAPOR DEPOSITED COATINGS

With physically vapor deposited (PVD) coatings there have been three distinct steps taken in the classification of thin film morphology (12). Movchan and Demchishin (13) were the first to classify thin films using a structure zone model (SZM). They observed that regardless of the thin film material, its morphological structure is related to a normalized, or reduced, temperature  $T/T_m$ , where  $T$  is the actual film temperature during deposition, and  $T_m$  is its melting point, both in K (12). They found that by increasing the deposition temperature, they could obtain at least three qualitatively distinct structure zones (Figure 8). Zone 1 in their classification consists of tapered columns with domed tops and is in a region of low adatom mobility. In zone 2, the structure is of a straight columnar nature and has a smooth surface morphology. For zone 3 the physical structure resembles equiaxed crystallites, much the same as those found in recrystallized metals.

Unlike Movchan and Demchishin (13) who prepared their films by electron beam evaporation, Thornton (14,15) used magnetron sputtering and introduced a new parameter, the sputtering gas pressure. He showed that both  $T/T_m$  and the sputtering gas pressure have an identifiable and significant effect on thin film growth (12). Thornton's model includes a fourth transition zone, called zone T, between zones 1 and 2 (Figure 9). In this zone the films have a smoother surface morphology and are denser than films from the surrounding zones (12).

Recently, Messier and colleagues, have shown that the physical structure of thin films changes as a function of thickness (12,16-19). A distribution of sizes from the smallest clustered units ( $\mu\text{m}$ -sized) to the largest, dominant sizes perceived, typically  $\mu\text{m}$ -size units in SEM micrographs, is the resulting structural heterogeneity (16). Thornton's model is essentially retained in this new SZM which includes the similarity in morphology of various levels of magnification as well as the evolutionary growth of morphology (17). A revised SZM model for zone 1 structures is shown in Figure 10, wherein all the distinct levels of physical structure column/void sizes are considered and assigned subzones 1A, 1B, 1C, 1D and 1E (17). The smallest size level (1-3  $\mu\text{m}$ ) is represented by zone 1A and the largest by zone 1E (300  $\mu\text{m}$  column sizes). Larger sizes can be assigned designations of 1F, 1G, etc. This structure is not unique to the deposition technique but has been found in all vapor deposited films, as well as electrodeposited films (12,18). This universality in the physical structure of a variety of materials and self-similarity in structural evolution indicates a common origin of thin film growth and a possible fractal description (12,16,18,19). Fractals are discussed later in this chapter.

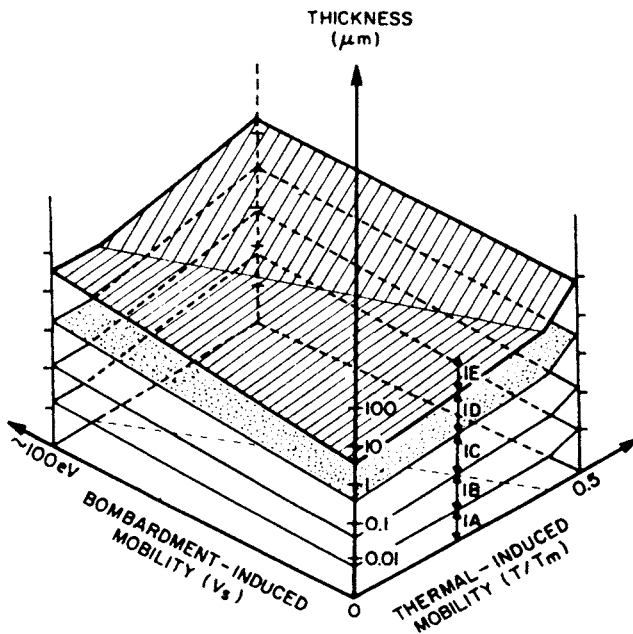


**Figure 10:** Revised structure zone model for films. From Messier, Giri and Roy, reference 17. Reprinted with permission of the American Vacuum Society.

## INFLUENCE OF SUBSTRATE

The structure of most electrodeposits is determined by epitaxial and pseudomorphic growth onto a substrate and by the conditions prevailing during deposition. Typically, a deposited metal will try to copy the structure of the substrate and this involves epitaxy, which occurs when definite crystal planes and directions are parallel in the deposit and substrate, respectively (1,20). Epitaxy is the orderly relation between the atomic lattices of substrate and deposit at the interface, and is possible if the atomic arrangement in a certain crystal direction of the deposit matches that in the substrate. Another term, pseudomorphism, refers to the continuing of grain boundaries and microgeometrical features of the cathode substrate into the overlying deposit. A deposit stressed to fit on the substrate is said to be pseudomorphic (20). Pseudomorphism persists longer than epitaxy.

The structure of a deposit and its properties and adhesion can be noticeably influenced by the substrate upon which it is plated. Figure 11 shows cross sections of copper electrodeposited on cast copper (9). If the substrate was cleaned but not pickled prior to plating, the structure of the plated deposit was quite different (fibrous) compared to that of the cast copper (coarse grained), Figure 11a. However, use of pickling after cleaning resulted in a structure wherein the copper crystals were continuations of the crystals in the copper basis metal (Figure 11b). Such reproductions of the basis metal structure may occur even with dissimilar metals that may vary appreciably in lattice structure and spacing (21).

The effect of the type of substrate on the properties of nickel electrodeposited on as-rolled and on annealed, cube-textured copper sheet is shown in Table 2. The influence of the small grain size induced in the deposits plated on the as-rolled sheet is apparent in the higher strength and ductility, compared with the deposit plated on the annealed, cube textured sheet which was coarse-grained (22).

Figures 12 and 13 show the influence of substrate on elongation of copper deposited from an acid sulfate solution (23). With 304 stainless steel as the substrate, the elongation of the copper was highly irreproducible and drifted alternately between high and low values (Figure 12). Acceptably reproducible results were obtained with a much more corrosion resistant substrate, Inconel 600 (Figure 13).

## PHASE TRANSFORMATIONS

A phase transformation is a change in the number or nature of phases as a result of some variation in the externally imposed constraints such as the temperature, pressure, or magnetic field. As will be shown in

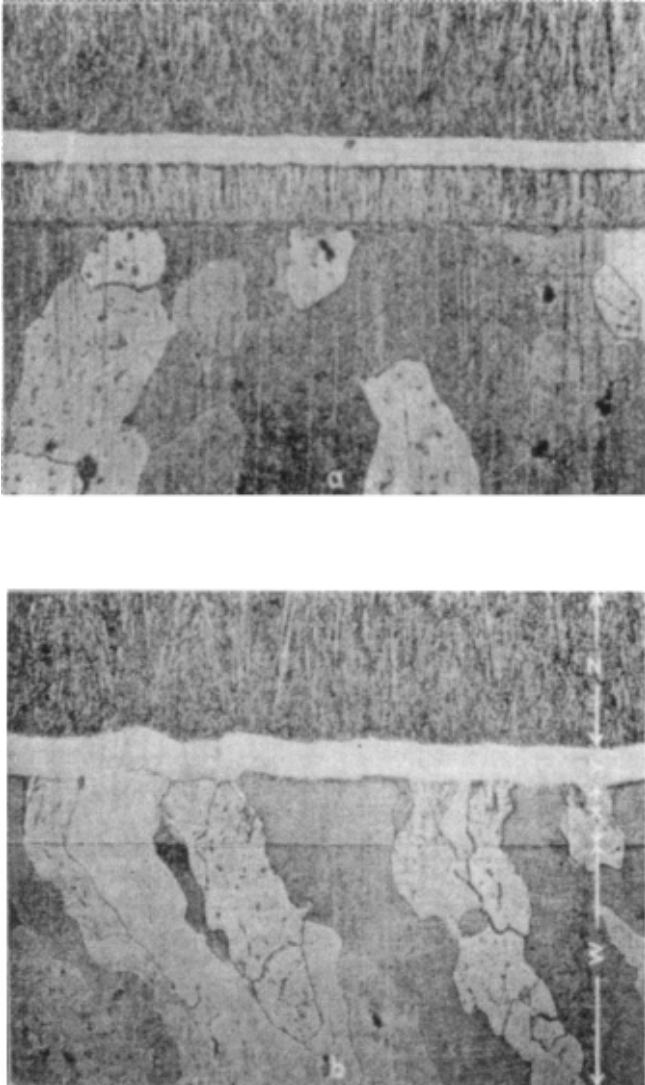


**Figure 11:** Cross section of the chilled side of cast copper, upon which copper was electrodeposited. (a) The surface was cleaned, but not pickled prior to electroplating. (b) The surface was pickled (bright-dipped) after cleaning. The various zones in (b) also apply to (a), i.e., W, the base metal; X, the electrodeposited copper (first layer); Y, electrodeposited nickel; and Z, electrodeposited copper (second layer). Reprinted with permission of McGraw-Hill, Inc.

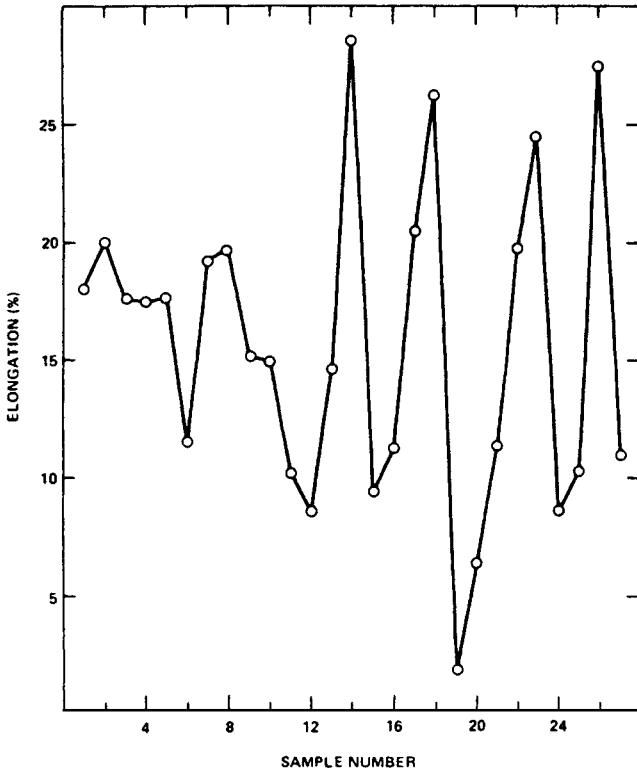


**Figure 12:** Measured elongation for a series of deposits plated on a rotating (750 rpm) 304 stainless steel mandrel from an acid copper sulfate solution containing 5 ml/l CUBATH M HY additive (Oxy-Metal Industries). Deposit thickness was 50  $\mu\text{m}$  (2 mils). From reference 23. Reprinted with permission of American Electroplaters & Surface Finishers Soc.

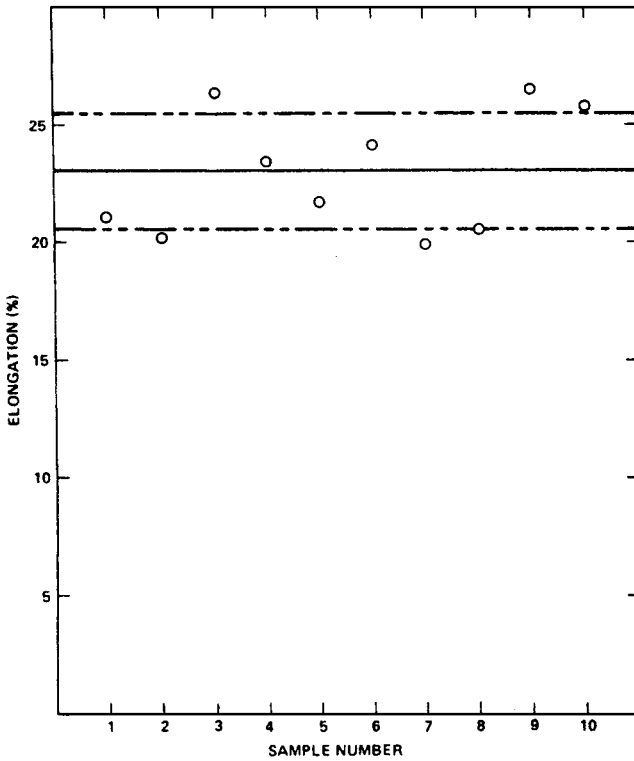


**Figure 13:** Elongation for a series of deposits plated on an Inconel 600 mandrel under the same conditions as Figure 12. From reference 23. Reprinted with permission of American Electroplaters & Surface Finishers Soc.

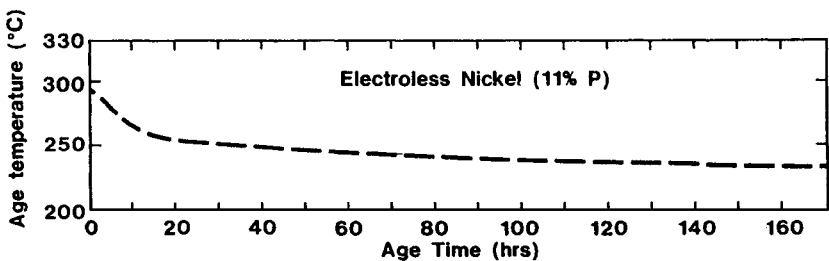


**Figure 14:** Time/temperature profile illustrating the transition from an amorphous to a crystalline structure for electroless nickel containing 11% (wgt) phosphorus. Adapted from reference 29.

**Table 2 - Effect of Substrate on Properties of Electroplated Nickel\* (from Reference 22)**

Material	Composition	Young's Modulus GPa	Yield Strength MPa	Tensile Strength MPa	Percent Elongation
Ni plated on as- rolled Cu	Ni	104	215	382	2.2
		5**	6	34	0.3
Ni plated on cube- textured Cu	Ni	104	120	222	7.1
		4**	3	7	0.5

\* Nickel was plated in an all-sulfate solution at a current density of 2.5 mA/cm<sup>2</sup> to a thickness of about 10 μm.

\*\* Values in this line are standard deviations.

the following examples, such changes in the nature of either a substrate or a coating after being deposited on a substrate can noticeably affect properties.

### A. Electroless Nickel

As-deposited electroless nickel is metastable and undergoes a crystalline transition at moderate temperature (240 to 400°C). This change causes a rapid increase in the hardness and wear resistance of the coating while reducing the corrosion resistance and ductility (24,25). The transition also causes an increase in density and accordingly a decrease in volume. This volume change, which can vary from 0.1% to 1.3% (26-28), coupled with differential thermal expansion, is the cause for cracking or fissuring often found in deposits after heat treatment (28). The extent of the crystalline transition is a complex function of a number of factors including: 1) temperature and time at temperature, 2) heating rate, 3) previous temperature history, and 4) phosphorus content (29). Figure 14 provides a time/temperature profile which illustrates the transition from an amorphous to a crystalline structure for electroless nickel containing 11% phosphorus. If thermal exposure is maintained in the time/temperature envelope below the dotted curve, then the electroless nickel will remain entirely amorphous. However, if exposure conditions fall above this curve, then partial or complete crystallization will occur (29).

## B. Gold-Copper

The gold-copper system exhibits disorder-order transformation and the strengthening mechanism of these electrodeposited alloys is associated with this phenomenon. A 50 at% Au-Cu (75 wt% Au) alloy has a face centered cubic structure in the disordered state. In the ordered condition it has a tetragonal structure. During transformation there is a volume decrease which results in the formation of lattice strains. Increases in mechanical strength during heat treatment correlate with increases in coherency strains between ordered nuclei and disordered matrices (30). Longer annealing times eliminate these strains by microtwinning and result in decreases in mechanical strength. Typical results obtained with gold-copper electrodeposited alloys are shown in Figure 15.

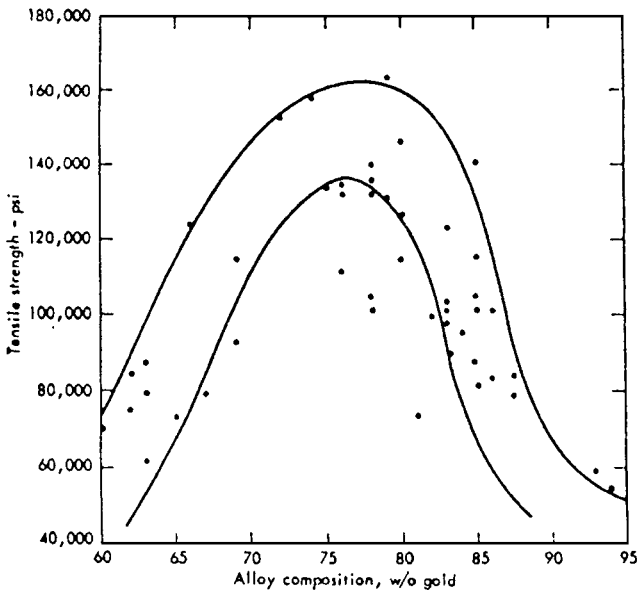


**Figure 15:** Effect of heating for 3 hours at 350°C on the tensile strength of electroformed gold-copper alloy. From reference 30. Reprinted with permission of American Electroplaters & Surface Finishers Soc.

## C. Transformation in Tin-Nickel

Electrodeposited tin-nickel (NiSn) is another example of a deposit that undergoes a transformation upon heating. This phase change causes cracking and exfoliation of the coating, so that while actual melting

of the deposit does not take place below about 800°C, the electrodeposited material cannot be safely used at temperatures above about 250°C (31). NiSn transforms to Ni<sub>3</sub>Sn<sub>2</sub> and Ni<sub>3</sub>Sn<sub>4</sub> when isothermally heated at 300°C for at least 20 hours and when isothermally heated at and above 400°C for at least 1 hour. The deposit has been shown to be stable at room temperature for at least 10 years (32). It is not recommended as a diffusion barrier for parts subjected to high temperatures. For example, tin-nickel deposits 12.5 and 2.5 μm thick, deposited as a diffusion barrier between 60 μm fine gold and copper showed decomposition into discrete particles after only 50 hours exposure at 500°C. Gold and copper completely penetrated the original tin-nickel layer as if it were not even present(33).

#### D. Palladium

An unstable thermodynamic phase resulting from high hydrogen in the lattice can cause cracking of palladium deposits during or after plating thus exposing the less noble substrate and significantly reducing corrosion performance (34,35). The key is keeping the H/Pd ratio below 0.03 since in this range palladium hydride is present in an α phase with a lattice constant close to that of pure Pd. Escape of hydrogen from this structure does not cause any lattice distortion. When the H/Pd ratio is above 0.57 palladium hydride is present in a β phase with a lattice constant which is about 3.8% higher than that of the α phase. The β phase is thermodynamically unstable and converts to α phase with the release of hydrogen and causes a contraction of the lattice and cracking of the deposit. Deposits with a H/Pd ratio between 0.03 and 0.57 have a combination of α and β phases and since the β phase causes problems, the way to avoid subsequent cracking of deposits is to keep the H/Pd ratio below 0.03.

#### E. Cobalt

Cobalt exhibits an unusual structural transformation (fcc → hcp) as a result of hydrogen inclusion and subsequent outdiffusion. A peculiar feature of cobalt deposits is that a high temperature phase (>417°C) can be obtained by deposition at ambient temperature. This "fcc cobalt" is produced in a solution with a pH less than 2.4 by the simultaneous incorporation of hydrogen to form an "fcc cobalt hydride". Since this hydride is unstable at ambient temperatures, it decomposes into basic cobalt (hcp) during the outdiffusion of hydrogen. At high pH (>2.9), stable hcp cobalt is obtained (36). Incorporation of hydrogen and hydroxide also significantly alters the microstructure of nickel deposits (37).

## F. Miscellaneous

The bores of many cannon tubes are electroplated with chromium to provide better resistance to erosion, wear and corrosion resistance (38). In fact, the resistance of the chromium deposit to erosion and wear is so good that there is little or no wear of the bore until the chromium begins to spall off the steel substrate. This spalling appears to chiefly be the result of the underlying steel undergoing a phase transformation with an attendant volume increase. It has been found that if the electroplate is made thicker, the underlying steel never reaches the transformation temperature and the useful life of the plated cannon is considerably increased (38).

Metal surfaces exposed to gas may undergo transformation, with deterioration of their properties. The rate of the phenomenon depends largely on the nature of the metals, the attacking gases, and the new products that may form at the interface between the two phases (39). One example is silicon which upon oxidizing to  $\text{SiO}_2$  undergoes expansion resulting in highly compressive stresses on its surface (40).

## MICROSTRUCTURAL INSTABILITY AT ROOM TEMPERATURE

### A. Copper

The metallurgical instability of some copper deposits can create problems when this material is used for optical applications. Copper deposits have been shown to markedly soften after storage at room temperature for 30 days (41). Another example relates to copper mirrors which revealed a change in their optical surfaces over a period of six months. This was caused by recrystallization which had occurred in the copper attendant with a shifting of the surface along individual grain boundaries (42). More information on this is presented later in this chapter in the discussion on texture. After recrystallization, an orange-peel effect is visible to the eye in some cases. Figure 16 shows a diamond turned copper surface before recrystallization and Figure 17 shows a surface after recrystallization. The problem is caused by the high density of defects in the electroplated copper, often much higher than that achieved by cold working (discussed in more detail in the chapter on Properties). With copper, the problem is exacerbated by lower current densities (less than 20 asf).



**Figure 16:** Normarski micrograph of a diamond turned copper surface before recrystallization (100  $\times$ ). From reference 42. Reprinted with permission of the American Electroplaters & Surface Finishers Soc.

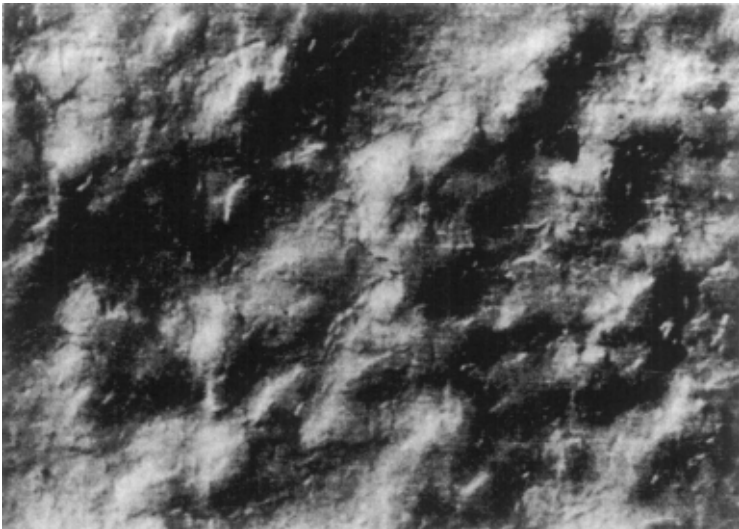


**Figure 17:** Normarski micrograph of a diamond turned copper surface after recrystallization (100  $\times$ ). From reference 42. Reprinted with permission of the American Electroplaters & Surface Finishers Soc.

Differential scanning calorimetry (DSC)<sup>1</sup> reveals that copper plated at 5 asf has a very high recovery energy at 148°C and a much lower recrystallization energy exotherm at 284°C (Figure 18, Ref. 42). By comparison, copper plated at 15 asf shows a joined recovery/ recrystallization energy exotherm at 306°C (Figure 19). The way to eliminate the recrystallization problem at room temperature is to heat treat at a low temperature (1 hour at 250°C). This removes the recovery energy and no recrystallization and grain growth occurs (42). Figure 20, a DSC of copper plated at low current density (5 asf) and then heated for 1 hour at 250°C, shows no retained recovery energy and a reduction in the recrystallization energy.

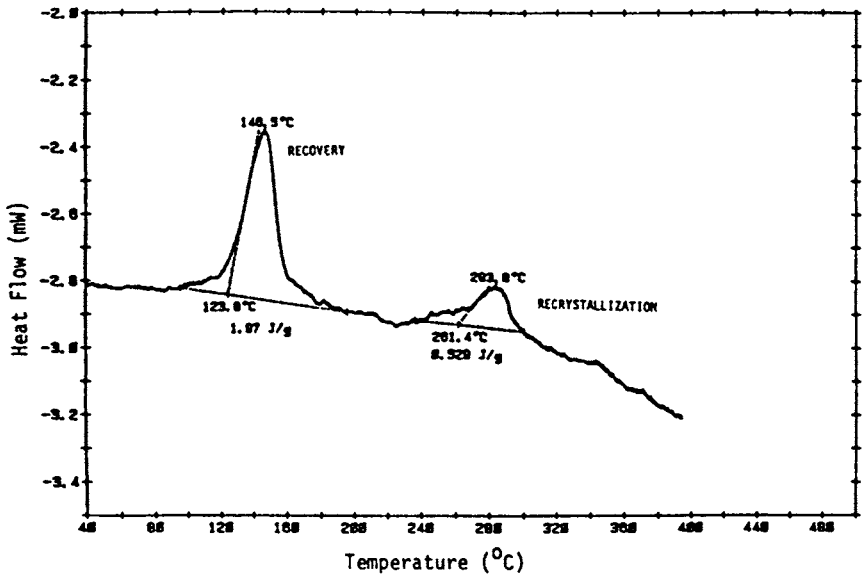


**Figure 18:** Differential scanning calorimetry plot showing two exotherms for copper plated at 5 asf. From reference 42. Reprinted with permission of the American Electroplaters & Surface Finishers Soc.

<sup>1</sup> Differential scanning calorimetry (DSC) measures the heat absorbed or released by a substrate as it passes through transitions or undergoes reactions. DSC can pinpoint the exact temperature or time in a process when a material goes through a transition, when it occurs, and where decomposition occurs.

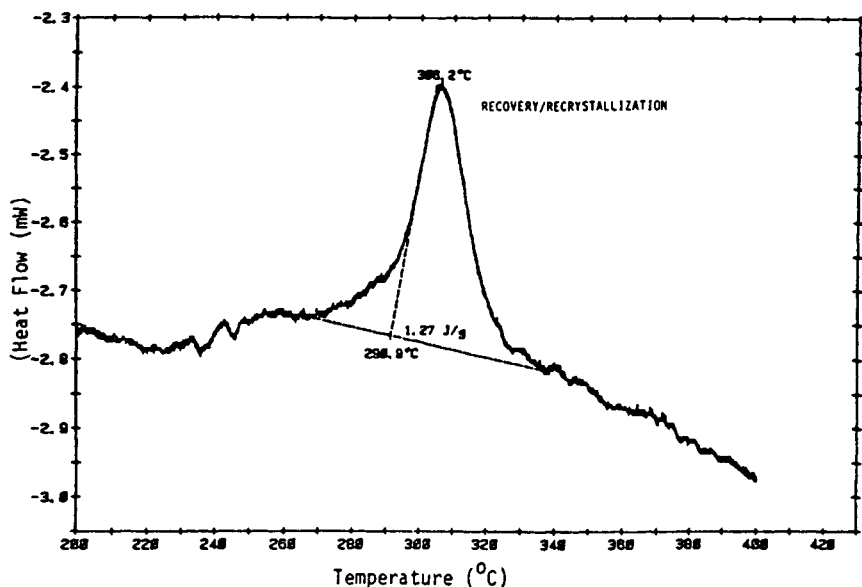


**Figure 19:** Differential scanning calorimetry plot showing energy release for copper plated at 15 asf. From reference 42. Reprinted with permission of the American Electroplaters & Surface Finishers Soc.

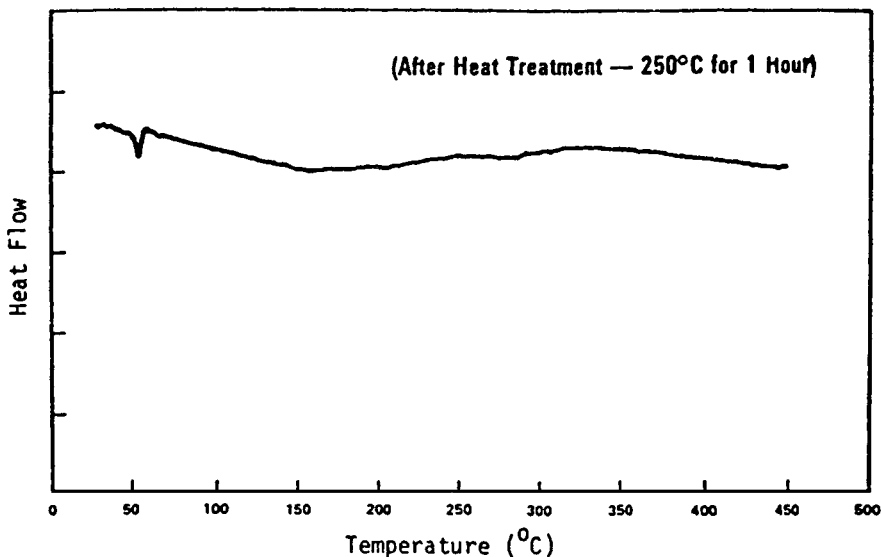


**Figure 20:** Differential scanning calorimetry plot of copper plated at 5 asf and then heat treated. From reference 42. Reprinted with permission of the American Electroplaters & Surface Finishers Soc.

## B. Silver

A silver flat mirror turned to better than 0.5 fringe deformed 9 fringes in 15 months after machining. This was due to room temperature creep (relief) of the silver electroplating stress. Other examples are brass mirrors which had been diamond turned flat, checked in an interferometer and electroplated with silver. The plating operation caused them to deform by 10 fringes. Removing the silver by machining eliminated the distortion and essentially restored the original features. The problem was eliminated by heat treating copper or silver plated parts at 150°C for 1 hour prior to diamond turning (43). Table 3 shows that some silver deposits exhibited a significant decrease in hardness as a function of time at ambient temperature after plating. This decrease in hardness has been attributed to recrystallization and grain growth(44).

**Table 3 - Hardness of Electrodeposited Silver from Cyanide Electrolytes as Related to Storage Time Versus Solution Additive<sup>(a)</sup>**

Solution Additive	Deposit Hardness (VHN)				
	Initial	1/2 Mo.	1 Mo.	3 Mo.	6 Mo.
None	110	105	102	100	90
Carbon	148 <sup>(b)</sup>	--	135	130 <sup>(b)</sup>	130
Disulfide, 1-1/2 ml/l					
Sodium Selenate, 0.8 g/l	125	124	107	65	66
Potassium Sulfate, 50 g/l	140	132	105	95	85
Cobalt, 1.7 g/l	108	98	87	84	88

(a) From reference 44; the solutions contained 26 to 30 g/l silver, 20 to 42 g/l free potassium cyanide and 30 to 34 g/l potassium carbonate. Plating current density was 21.5 A/m<sup>2</sup>.

(b) Grain size increased from 2.36 to 3.22 x 10<sup>-6</sup>cm during three months storage.

## TEXTURE

Texture, which is preferred distribution of grains (individual crystallites) having a particular crystallographic orientation with respect to a fixed reference frame, is an important structural parameter for bulk materials and coatings (45,46). It can noticeably affect a variety of functional properties which will subsequently be discussed and is an excellent materials science example illustrating how properties can be tailored. However, before discussing texture in detail, a brief review on crystallography is in order. It is convenient to be able to specify certain planes in crystal lattices and there are sets of conventional descriptors for this (4,20,47). Parentheses (100) around Miller indices signify a single plane or set of parallel planes. Curly brackets or braces {100} signify planes of a "form" - those which are equivalent in the crystal - such as the cube faces of a cubic crystal. To distinguish the notation for a direction from that of a position, the direction integers are enclosed in square brackets [100]. A set of directions which are structurally equivalent and called a family of directions is designated by angular brackets <100> (4,47). The three most important planes are {100}, {110} and {111} shown for cubic lattices by the hatched lines in Figure 21, which also includes the three most important directions, namely, <100>, <110>, and <111> (20).

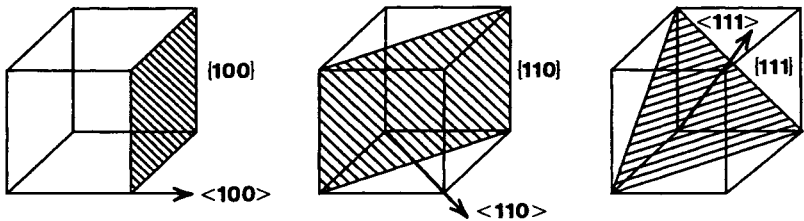


**Figure 21:** Crystal planes and directions. (a) {100} planes are faces of the cube, <100> directions are cube edges. (b) The sides of {110} planes are two face diagonals and two cube edges, <110> directions are face diagonals. (c) The sides of {111} planes are face diagonals, <111> directions are cube diagonals. One plane of each type is shown hatched. One direction of each type is shown by an arrow. Adapted from reference 20.

Table 4, which lists textures of coatings produced by various techniques, reveals that texture is highly dependent on the coating process used. For that matter, textures of electroplated coatings can be markedly influenced by solution composition and operating conditions. Examples include Pd, Ni and Au. With Pd, the texture of coatings for an identical

coating composition can be totally different and vary from textureless to a pronounced (111) or (110) texture or a combination of (111), (100), (211) and (110) components (45). Depending on pH and current density, five different textures can be obtained from a Watts nickel plating solution as shown in Figure 22 (48). Gold coatings produced on a rotating disc electrode in a cyanide solution show a variety of textures as an influence of current density and deposition rate (Figure 23a). Codeposition of particulates with the gold deposit shifts the texture domains (Figure 23b) thus indicating that composite layers have their own structural properties (45).

**Table 4 - Texture of some coatings produced by various techniques\***

Process Material	Electro- deposition (25-100°C)	PVD (200-400°C)	CVD (>500°C)
Ag	(111),(100)	(111)	
Cr	(111),(100)	(110)	
Fe	(111),(100)	(211)	
Au	(111),(211)	(111)	
NiFe	(111),(100)	(111)	
TiN		(111),(200)	
TC		(111),(100)	(110)(111)(200)

\* From reference 45

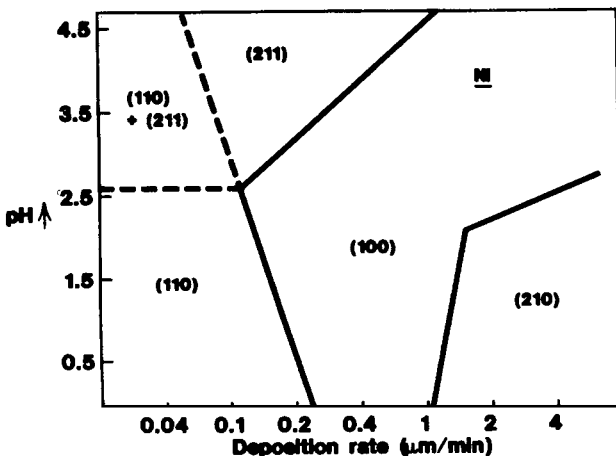


**Figure 22:** Texture stability diagram for nickel deposited in a Watts solution. Adapted from reference 48.

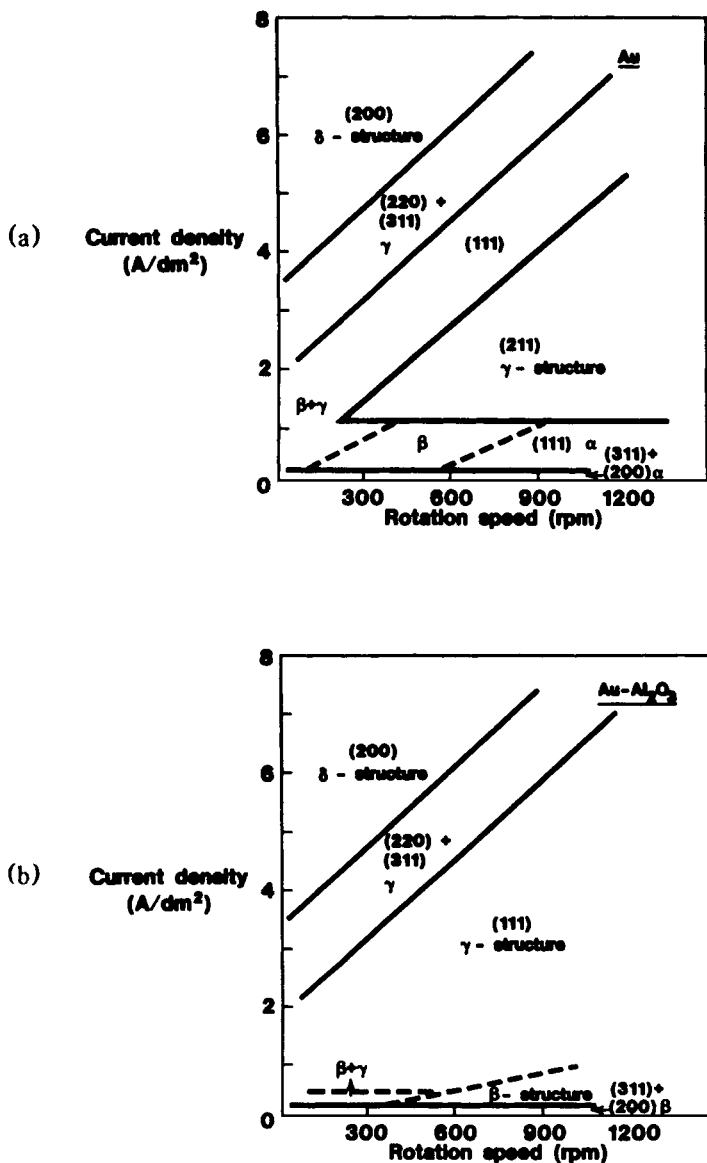


**Figure 23:** Texture stability diagrams for (a) pure gold coatings produced in a cyanide solution and (b) composite gold coatings. Adapted from reference 45.

Texture is completely independent of the substrate orientation for thick deposits (several  $\mu\text{m}$  or  $10\ \mu\text{m}$ , depending on plating conditions) (48). Electrochemical parameters appear to be the only governing factor. For example, texture mainly depends on cathodic potential and pH of the solution for a given electrolyte composition. This also applies to current density if temperature is kept constant (48). Some information on substrate texture and electroplated metal textures is shown in Table 5. This reveals that electrodeposits have the  $\langle 111 \rangle$  direction normal to the surface for BCC crystal structures and the  $\langle 110 \rangle$  direction for FCC substrates, independent of substrate orientation. With hexagonal closed packed metals such as zinc, the  $\langle 10\bar{1}2 \rangle$  direction is predominant and with tetragonal metals such as tin, the  $\langle 231 \rangle$  direction is preferred (49).

In the case of physical vapor deposition, the deposition rate directly determines the texture of coatings (45). For example, with HfN coatings, a distinct change from a predominant (111) to a (311) texture is noticed with increasing deposition rates (49,50).

**Table 5 - Relationship between the Substrate and the Electroplated Metal Textures<sup>(1)</sup>**

<u>Crystal Structure</u>	<u>Substrate Texture</u>	<u>Electroplated Metal Texture</u>
BCC	Cu $\langle 110 \rangle$	Fe $\langle 111 \rangle$
	Cu $\langle 111 \rangle + \langle 110 \rangle$	$\langle 111 \rangle$
	Au $\langle 111 \rangle$	$\langle 111 \rangle$
FCC	Ni $\langle 110 \rangle$	Cu $\langle 110 \rangle$
	Au $\langle 111 \rangle$	$\langle 110 \rangle$
	Fe $\langle 111 \rangle$	$\langle 110 \rangle$
Hexagonal Close Packed	Fe $\langle 100 \rangle$	Zn $\langle 10\bar{1}2 \rangle$
	$\langle 110 \rangle$	$\langle 10\bar{1}3 \rangle$
Tetragonal	Cu $\langle 111 \rangle + \langle 100 \rangle$	$\beta\text{-Sn } \langle 231 \rangle$
	Au $\langle 111 \rangle$	$\langle 231 \rangle$

(1) From Reference 49.

## INFLUENCE OF TEXTURE ON PROPERTIES

Texture can noticeably affect a variety of properties such as formability, corrosion resistance, etching characteristics of copper foil, paint adhesion on zinc, contact resistance, magnetic properties, wear resistance, porosity, and hardness of copper deposits. Examples will be discussed in the following sections.

### A. Formability

Electrogalvanized (zinc plated) steel is used by the automotive industry to improve the corrosion resistance of body panels. The sheet is exposed to a variety of processes during manufacturing. These include blanking, forming, spot welding, phosphating, and painting. A deposit structure compatible with these processes is crucial to the success of industrial electrogalvanizing. By adjusting the plating parameters to impart a desirable texture to the zinc layer, formability of electrogalvanized steel can be improved and cracking of the deposit prevented.

Plastic deformation in crystalline solids involves slip which is the displacement of one atom over another by dislocation movement. The major slip plane for zinc, which has a HCP lattice, is the basal plane (0001). In this plane, slip is at least 30 times easier than for any other in the HCP system (52,53). Basal plane deposits which are plastically deformed would exhibit elongation of individual grains, causing one layer of grains to slide over the next as shown in Figure 24a. Continuity of the coating is preserved by this action and this is essential for corrosion resistance. With prism-plane (10 $\bar{1}$ 0) deposits, fracture would likely occur since the stress is normal to the slip plane (Figure 24b). Results of drawbead tests show the fracture that is dominant in pyramid plane deposits which exhibit a pattern of parallel cracks normal to the draw direction. As shown in Figure 25, the deposit with the basal planes aligned parallel with the substrate exhibited good ductile elongation while the deposit with the basal planes nearly normal to the steel cracked under the same deformation (54,55). In practice the results aren't quite so simple since the stamping section is deformed by convex bending, concave bending and stretching (54). For more detail on texture and formability of zinc coated steel see references 46 and 56.

Plating experiments have revealed that pH strongly influences orientation of zinc deposits while temperature has a lesser effect (Table 6). The influence of flow rate is negligible (54).

### B. Corrosion

A metal surface is a complex of crystal faces, edges, corners,

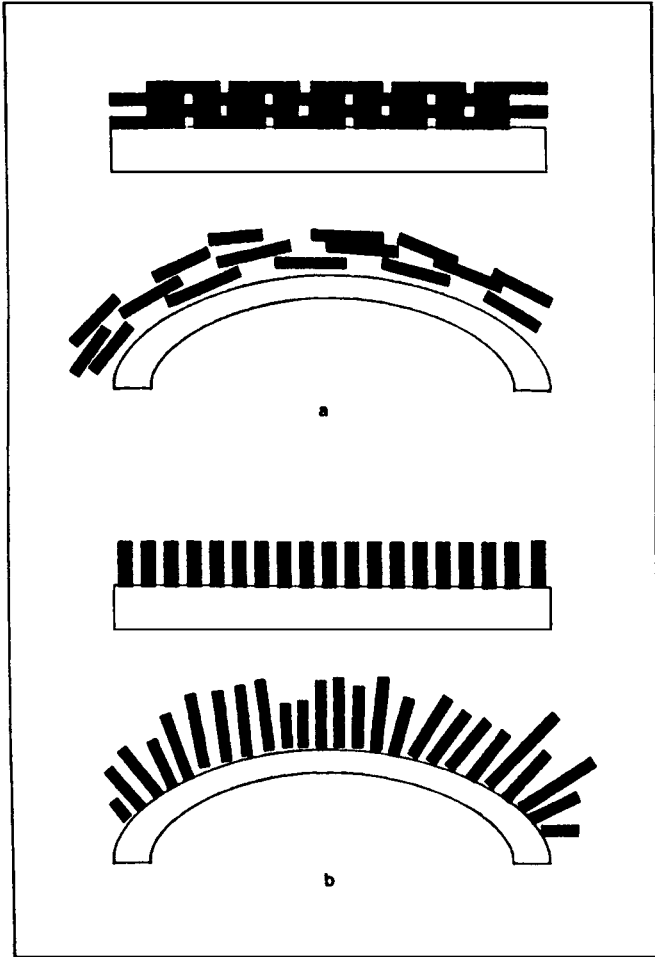


**Figure 24:** Consequences of simple tensile bending on deposits of (a) complete basal (0001) and (b) prism ( $10\bar{1}0$ ) plane orientation. From reference 54. Reprinted with permission of the American Electroplaters & Surface Finishers Soc.

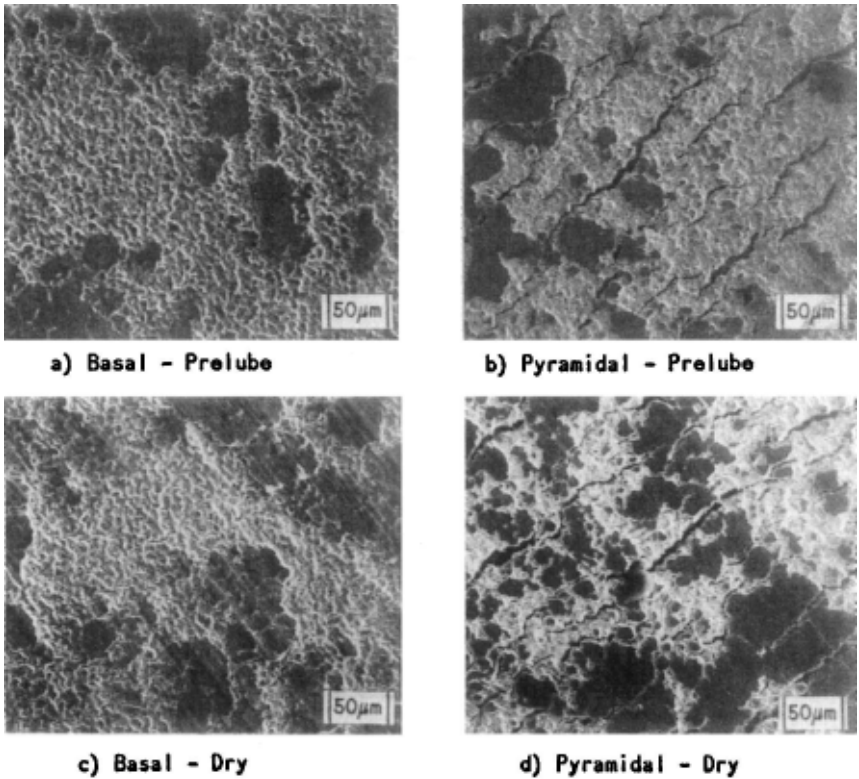


**Figure 25:** SEM photographs showing orientation groups of electrogalvanized zinc surfaces after drawbed tests: (a) basal, prelube; (b) pyramidal, prelube; (c) basal, dry; (d) pyramidal, dry. From reference 54. Reprinted with permission of the American Electroplaters & Surface Finishers Soc.

**Table 6 - Zinc Orientation Under Selected Deposition Conditions\***

Current density A/dm <sup>2</sup>	Temp C	pH	Basal (%) (0001)	Pyramidal(%) (101X)
150	50	3.0	80-95	5-20
150	50	4.2	>45	>45
50	26	3.5	>60	32
50	26	4.5	20	>75

\* From Reference 54

boundaries and disturbed layers (57). A composite of these various types of structure, in turn, dictates the properties of the surface. The change in free energy determines the reaction rate and this varies with the crystal face because the arrangement of atoms is different with different crystal faces. For example, with tungsten the ratio of free energies between two faces may in some cases be as high as a factor of 5. A practical example of this is shown in Table 7 which lists the relative rates of etching on various faces of copper crystals by acids containing hydrogen peroxide. With the rate of attack on the (111) face taken as unity, it can be seen that the etching rate can vary by as much as a factor of almost 2 to 1 (57).

**Table 7. Relative Rates of Corrosion of Different Faces of Copper Crystals\***

	Crystal Face		
	(111)	(100)	(110)
0.3 N HCl -- 0.1 N H <sub>2</sub> O <sub>2</sub>	1	0.90	1.0
0.3 N Acetic acid -- 0.1 N H <sub>2</sub> O <sub>2</sub>	1	0.90	0.55
0.3 N Propionic acid -- 0.1 N H <sub>2</sub> O <sub>2</sub>	1	1.28	1.33

\* From reference 57

With nickel, the rate of anodic solution of different grains increases in the order (111) < (100) < (110) (58). With an increase in the degree of cold deformation there is an increase in the anodic current density in the active area (59).

The corrosion behavior of zinc alloy coatings is affected by texture in terms of the ability of the layer to act either sacrificially or as a protective corrosion barrier. For example, zinc grains with a near {0001} orientation have much lower corrosion currents in sodium hydroxide solutions than those of other orientations (60). Corrosion rate data in 0.5 N sodium hydroxide solution for polycrystal and oriented crystal specimens are shown in Table 8. The corrosion current rate decreased as the packing density increased (61). Others have also discussed the influence of texture on the corrosion of zinc deposits (54,62).

**Table 8 - Corrosion Potentials, Currents and Rates for Zinc\***

Exposed Crystal Plane	Corrosion Current $\mu$ amps/cm <sup>2</sup>	Calculated Corrosion Rate mil/year
(0001)	81	48
(10 $\bar{1}$ 0)	127	75
(11 $\bar{2}$ 0)	261	153
Poly-crystal	160	94

\* From Reference 61

### C. Etching Characteristics of Copper Foil

The simple etch process that has worked so well for years in printed wiring board fabrication is becoming less viable as geometries decrease due to the inherent undercut associated with the process. Isotropic etch processes deliver copper conductors having approximately trapezoidal cross sections and irregular widths (63). An anisotropic etch chemistry has been developed for producing straight sidewall etched structures with little or no line loss from copper foils which have a high (111) component. Figure 26 illustrates the relationship between line loss upon etching (undercut) and (111) content of the foil substrate (64). However, it's important to note that experiments with other types of copper foils showed that the correlation given in Figure 26 is only valid for copper foils electrodeposited on aluminum carriers. Copper foils prepared by other methods etched isotropically regardless of (111) content. X-ray pole figure analysis revealed significant qualitative structural differences between the anisotropically etching foils and the other high (111) foils which etched isotropically (63).

Others have reported that copper crystal orientation is only a factor in the definition of fine line features (3 mils or less) and that the best and worst foils relative to (111) content differed by at most 0.5 mils. This difference, in their observation, is negligible or becomes incorporated in other process variations when dealing with line widths of 4-5 mils, or greater (65).

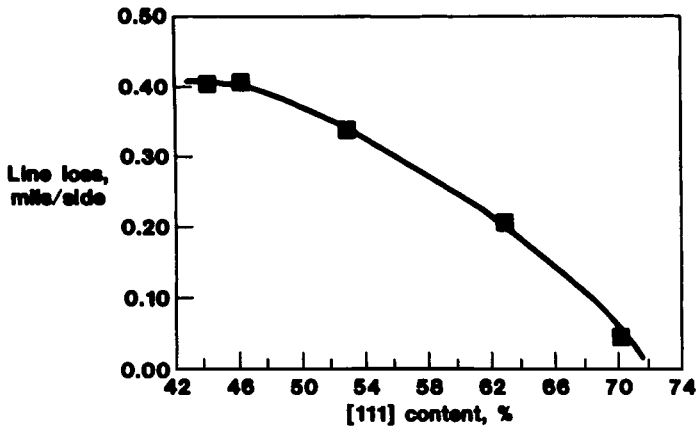


**Figure 26:** Relationship between line loss upon etching (undercut) and (111) content of copper foil. Adapted from reference 64.

#### D. Paint Adhesion on Zinc Coated Steel

Adhesion of paint to zinc coated steel is greatly affected by texture (66,67). Zinc grains with {0002} orientations parallel to the sheet surface provided better paint adherence than those of other orientations (Figure 27). This was related to two factors: 1) on deformation these grains would not yield in tension due to bending because the slip plane {0001} was parallel to the surface (the bending tension causes many small microcracks to occur in the zinc layer thus relieving residual stresses between the paint and zinc grains), and 2) zinc with a large fraction of {0001} oriented grains was more readily cleaned of contaminating organics that might have conceivably interfered with paint adherence (49,66,67).

#### E. Contact Resistance of Electroplated Nickel

Various nickel platings have been shown to provide surprisingly different contact resistances when exposed to the atmosphere for long periods of time (68). The only difference that could be observed among the various deposits was a variation in plating texture. Force vs. contact resistance curves for various orientations of single crystal nickel are shown in Figure 28 and verify that the difference in contact resistance can be explained by the orientation and its effect on oxide growth. Polycrystalline nickel electrodeposits were shown to behave similarly to single crystals, as

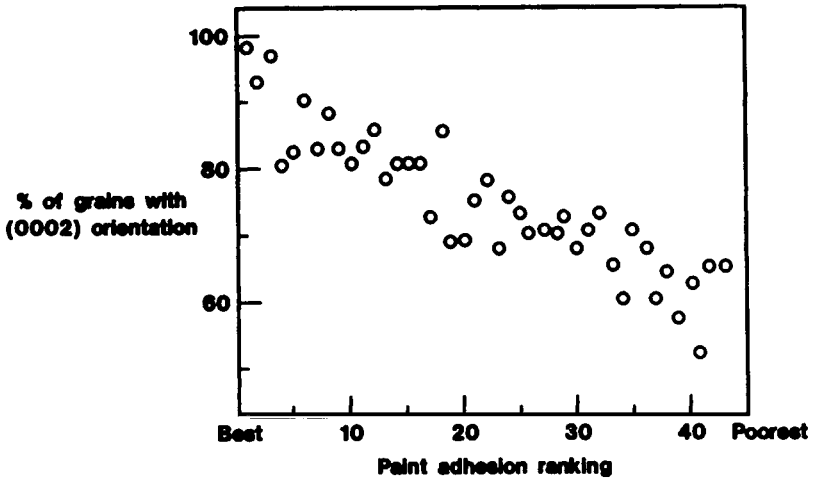


**Figure 27:** Relationship between the orientation of zinc and paint adhesion. Adapted from reference 67.

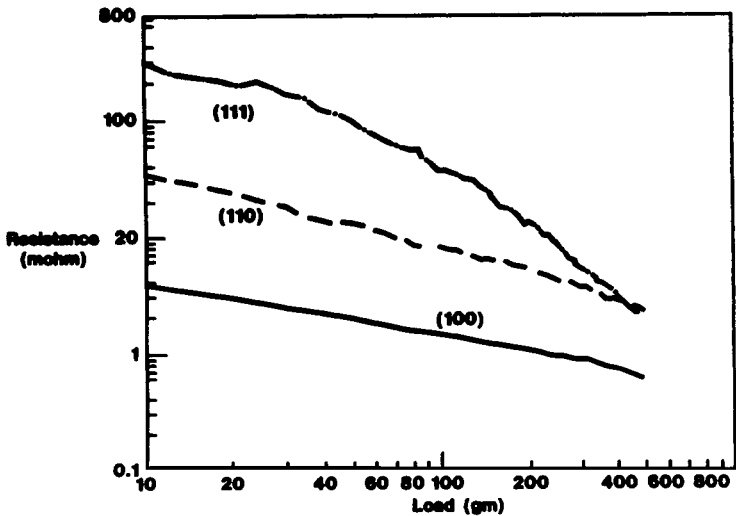


**Figure 28:** Resistance-force curves for three oriented nickel single crystal surfaces. Adapted from reference 68.

long as a majority of the grains were oriented with the {100} plane parallel to the surface. The oxidation rate of {100} oriented nickel single crystal surfaces was shown to be self limiting at room temperature. Figure 29, a probability plot of a heat age test, provides information on contact resistance. Change in resistance data are plotted as a cumulative percentage for three electrodeposits: nickel with a {100} texture, nickel with a {111} texture and gold. Ideal behavior would be represented by a horizontal line while deviations from this, particularly a significant upward trend, would indicate degradation. Figure 29 shows that nickel with a {100} texture behaves slightly better than gold plated samples and significantly better than {111} textured nickel (68).

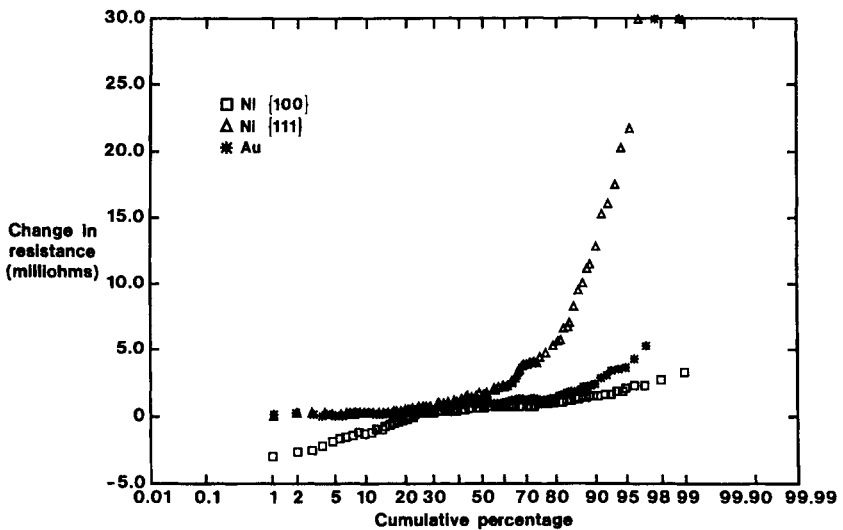


**Figure 29:** Change in resistance vs. cumulative percentage for {100} nickel, {111}, nickel, and gold after 103 days heat age testing. Adapted from reference 68.

## F. Magnetic Properties of Cobalt/Phosphorus Films

Electroless plated cobalt/phosphorus thin films are usually characterized by low to medium coercivity values (300-900 Oe). For some applications, it would be desirable to have films with coercivities greater than 900 Oe. Table 9 shows that films with minimum preferred orientation exhibit maximum coercivity values (69). The ratio of the intensity of the (002) and (101) diffraction rings changes with the hypophosphite concentration of the plating solution with zero preferred orientation obtained at solution hypo concentrations of 5-6 v/o.

**Table 9 - Influence of Solution Hypophosphite Concentration on Preferred Orientation and Magnetic Coercivity of Electroless Cobalt/Phosphorus Films\***

Solution hypophosphite concentration (v/o)	Preferred orientation (002)/(101)(%)	Hc (Oe)
5	0	1026
6	0	938
4	<10	930
3	<10	745
7	<10	461
2	>50	493
8	>50	200

\*From reference 69.

## G. Wear Resistance

With face centered cubic crystals the slip plane, which is the crystallographic plane in which adjacent atomic layers can slide over each other with minimum friction, is the (111). A face centered cubic electrodeposit such as palladium is typically (110) rather than (111) oriented and does indeed exhibit a large amount of wear when tested against itself in sliding friction. A (111) oriented deposit, produced by revising the brightener system exhibits superior wear performance (70). The wear resistance of ion plated TiN or TiC films is also related to preferred orientation, increasing as the intensity diffracted from the (111) plane becomes stronger (71,72).

## H. Porosity

Rates of pore closure and covering power for bright gold deposits on copper are related to the crystallographic orientation of the deposit. This is discussed in detail in the chapter on Porosity and also illustrated in Figures 13 and 14 in that chapter. Similar effects have been shown with palladium electrodeposits as indicated in Figure 30. The curve for the higher degree of preferred orientation (111), which for face-centered cubic palladium is the most densely packed, is displaced downwards indicating reduced porosity when compared with the deposit that is (110) oriented (70).

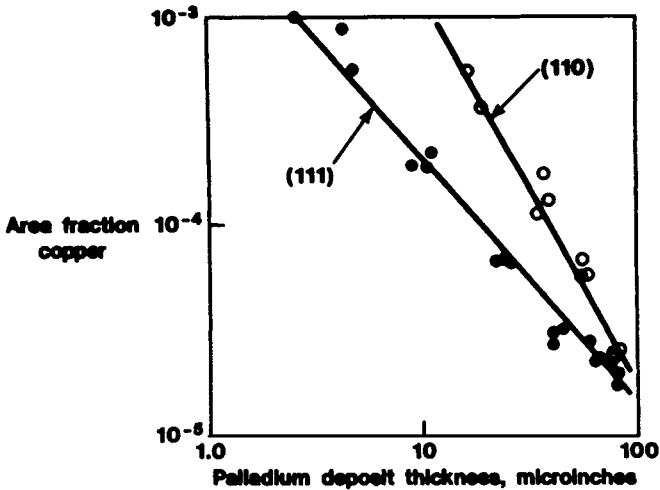


**Figure 30:** Porosity versus thickness plots for palladium electrodeposits from chelated solution on copper electrical terminals. Porosity measurements by corrosion potential in 0.1 M ammonium chloride. Adapted from reference 70.

## I. Electrodeposited Copper Recrystallization

The metallurgical instability of some copper deposits at room temperature was mentioned earlier in this chapter. As discussed in the chapter on Additives, organic addition agents are often used to help produce bright copper deposits. Components or break-down products from these additives can be incorporated in the deposit and provide specific growth orientation as well as stresses. In an effort to form a more thermodynamically stable structure, recrystallization is likely to occur (45,73). This recrystallization is accompanied by a texture evolution and well as a lowering of hardness as shown in Figure 31. The relationship between hardness and [111] content of a copper foil is shown in Figure 32.

## FRACTALS

### A. Introduction

Deposits produced in solutions containing no additives, particularly simple salt solutions, are often dendritic or treelike and aside from artistic uses, of no practical value until recently. Now these dendritic structures are playing an important role in the new science of fractals (74). Figure 33a shows the structure obtained in a zinc sulfate solution containing no

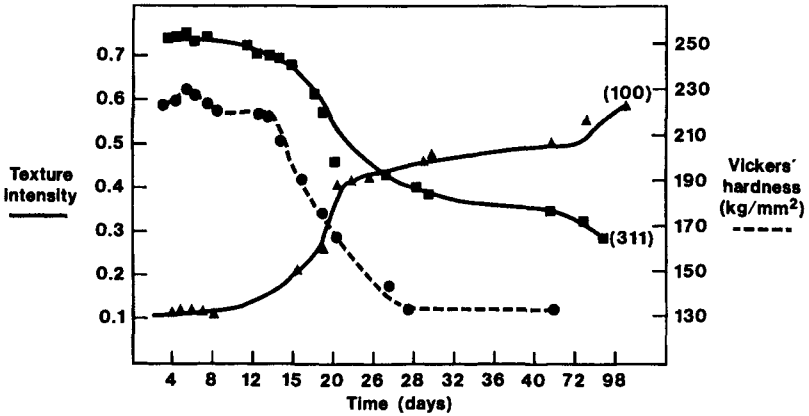


Figure 31: Change with time, at room temperature, of the intensity of texture components in copper electrodeposits. Adapted from reference 73.

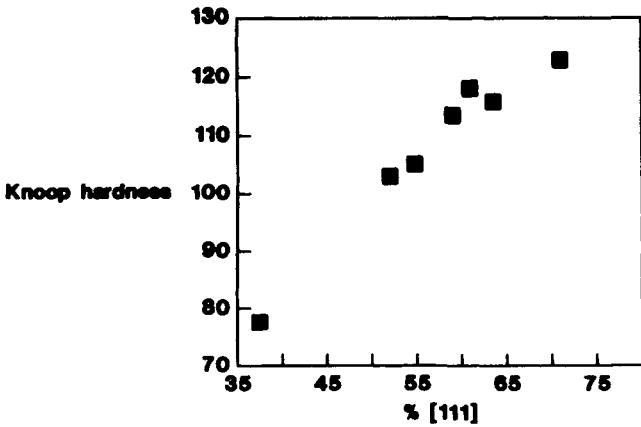
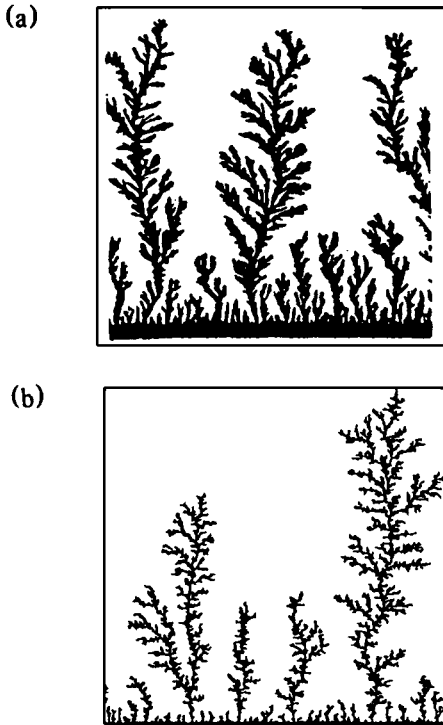


Figure 32: Relationship between Knoop hardness and the [111] content of copper foil. Adapted from reference 64.



**Figure 33:** (a) Electrodeposited clusters (about 5 mm long), photographed 15 min. after the beginning of the growth. (b) A diffusion-limited aggregate computed with a random walker model. The digitized images in both (a) and (b) have about  $1.6 \times 10^4$  boundary sites. From reference 74. Reprinted with permission of the American Physical Society.

additives, and Figure 33b a fractal "tree" grown by a computer algorithm called diffusion-limited aggregation. An interesting observation is that Figure 33b bears a striking resemblance to "trees" or "dendrites" produced by electrolysis in simple salt solutions (74).

A fractal is an object with a sprawling tenuous pattern (75). Magnification of the pattern would reveal repetitive levels of detail; a similar structure would exist on all scales. For example, a fractal might look the same whether viewed on the scale of a meter, a millimeter or a micrometer. Examples of fractals in nature include, formation of mountain ranges, ferns, coastlines, trees, branching patterns of rivers and turbulent flow of fluids or air (75,76). In the human body, fractal like structures abound in networks of blood vessels, nerves and ducts. Airways of the lung shaped by evolution and embryonic development, resemble fractals generated by a computer (77).

Although the entire field of fractals is still in its infancy, in many instances applying either theoretical fractal modeling and simulations or performing fractal analysis on experimental data, has provided new insight on the relation between geometry and activity, by virtue of the very ability to quantitatively link the two (78). For the physiologist, fractal geometry can be used to explain anomalies in the blood flow patterns to a healthy heart. Studies of fractal and chaos in physiology are predicted to provide more sensitive ways to characterize dysfunction resulting from aging, disease and drug toxicity (77). For the materials scientist, the positive aspect of fractals is that a new way has been found for quantitative analysis of many microstructures of metals. Prior to this only a quantitative description has been available. This offers the potential for a better understanding the origin of microstructures and the bulk properties of metallic materials (79).

Fractal geometry forms an attractive adjunct to Euclidean geometry in the modeling of engineering surfaces and offers help in attacking problems in tribology and boundary lubrication (80). Fractured surfaces of metals can be analyzed via fractal concepts (77,81-88). Interestingly, the term "fractal" was chosen in explicit cognizance of the fact that the irregularities found in fractal sets are often strikingly reminiscent of fracture surfaces in metals (81).

For the coater, besides the items mentioned above, fractal analysis provides another tool for studying surfaces and corrosion processes (89-91). As Mandelbrot, the father of fractal science, wrote, "Scientists will be surprised and delighted to find that not a few shapes they had to call grainy, hydralike, in between, pimply, ramified, seaweedy, strange, tangled, tortuous, wiggly, wispy, wrinkled and the like, can, henceforth, be approached in rigorous and vigorous quantitative fashion" (92,93). Note that many of these terms have at one time or another been used to describe coatings. A method for describing these terms in a quantitative fashion is becoming a reality. Regarding corrosion, profiles encountered in corrosion pitting have been reported to be similar to those enclosing what are known as Koch Islands. These are mathematical constructions which can be described by fractal dimensions, thus suggesting the application of fractal dimension concepts for description of experimental pit boundaries (91). For general reviews and more details on fractals, see references 75,92-97.

## **B. Fractal Dimension**

The following two paragraphs describing fractal dimension are from Heppenheimer, reference 98. "A fractal dimension is an extension of the concept of the dimension of an ordinary object, such as a square or cube, and it can be calculated the same way. Increase the size of a square by a

factor of 2, and the new larger shape contains, effectively, four of the original squares. Its dimension then is found by taking logarithms:  $\text{dimension} = \log 4 / \log 2 = 2$ . Hence, a square is two-dimensional. Increase the size of a cube by a factor of 3, and the new cube contains, in effect, 27 of the original cubes; its dimension is  $\log 27 / \log 3 = 3$ . Hence, a cube has three dimensions.

There are shapes-fractals-in which, when increased in size by a factor  $m$ , produce a new object that contains  $n$  of the original shapes. The fractal dimension, then is  $\log n / \log m$ -evidently the same formula as for squares or cubes. For fractals, for example, in which  $n = 4$  when  $m = 3$ , the dimension is  $\log 4 / \log 3 = 1.26181$ . A fractal dimension, in short, is given by a decimal fraction; that indeed, is the origin of the term fractal (98)."

The above discussion shows that fractals are expressed not in primary shapes but in algorithms. With command of the fractal language it is possible to describe the shape of a cloud as precisely and simply as an architect might use traditional geometry and blueprints to describe a house (93). A linear algorithm based on only 24 numbers can be used to describe a complex form like a fern. Compare this with the fact that several hundred thousand numerical values would be required to represent the image of the leaf point for point at television image quality (93).

All fractals share one important feature inasmuch as their roughness, complexity or convolutedness can be measured by a fractal dimension. The fractal dimension of a surface corresponds quite closely to our intuitive notion of roughness (97). For example, Figure 34 is a series of scenes with the same 3-D relief but increasing fractal dimension  $D$ . This shows surfaces with linearly increasing perceptual roughness: Figure 34(a) shows a flat plane ( $D \approx 2.0$ ), (b) countryside ( $D \approx 2.1$ ), (c) an old, worn mountain ( $D \approx 2.3$ ), (d) a young, rugged mountain range ( $D \approx 2.5$ ), and (e) a stalagmite covered plane ( $D \approx 2.8$ ).

### C. Fractals and Electrodeposition

Fractals could be of importance in the design of efficient electrical cells for generating electricity from chemical reactions and in the design of electric storage batteries (94). Studies on electrodeposition have become increasingly important since they offer the possibility of referring to a particularly wide variety of aggregation textures ranging from regular dendritic to disorderly fractal (99). The reason electrodeposition is particularly well suited for studies of the transition from directional to "random" growth phenomena is that it allows one to vary independently two parameters, the concentration of metal ions and the cathode potential (74). Much of the interest in this field has been stimulated by the possibilities

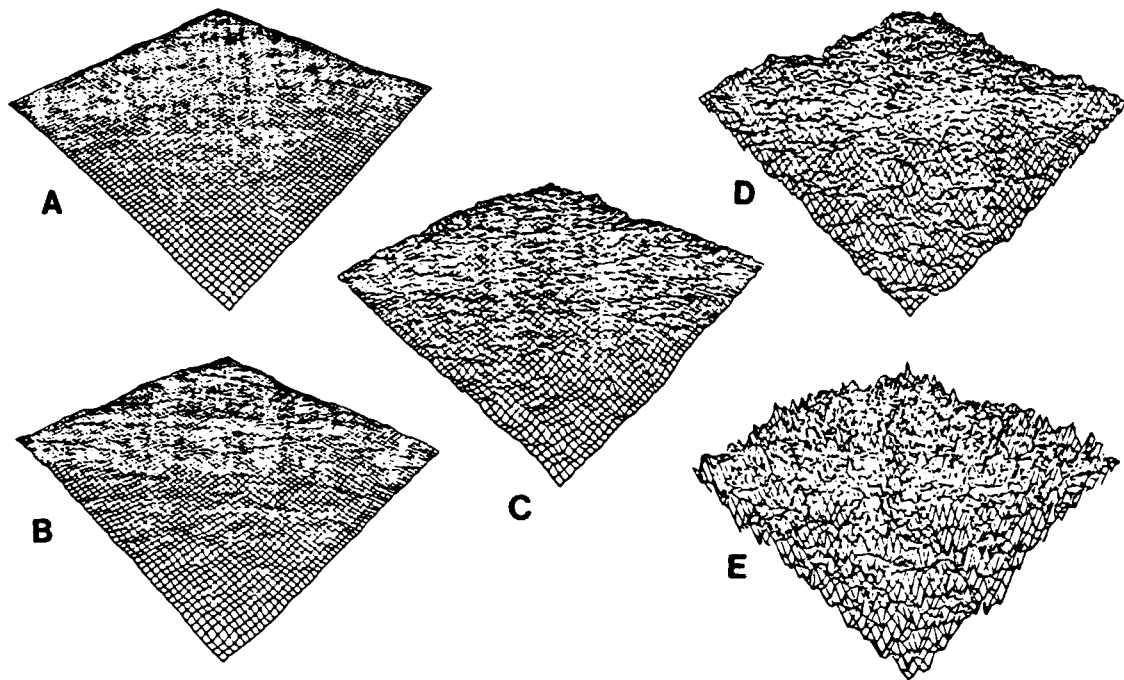


**Figure 34:** Surfaces of increasing fractal dimension. (a) = 2.0, (b) = 2.1, (c) = 2.3, (d) = 2.5 and (e) = 2.8. From reference 97. Reprinted with permission of IEEE.

furnished by real experiments on electrocrystallization for testing simple and versatile computer routines simulating such growth processes (74,75,-99-108). As mentioned earlier and shown in Figure 33, a deposit of zinc metal produced in an electrolytic cell has been shown to bear a striking resemblance to a computer generated fractal pattern. The zinc deposit had a fractal measured dimension of 1.7 while the computer generated fractal dimension was 1.71. This agreement is a remarkable instance of universality and scale-invariance. About 50,000 points were used for the computer simulation while the number of zinc atoms, in the deposit is enormously large, almost a billion billion (75).

#### D. Surface Roughness

Surface roughness is the natural result of acid pickling and abrasive cleaning processes in which, etched irregular impressions or crater like impressions are created in the substrate surface. At present, the effect of surface roughness on the service life of many coating systems is not well understood (109). In some cases, a rough surface may improve the adhesion as discussed in the chapter on Adhesion. In other cases, a rough surface may be detrimental in that it may affect the electrochemical behavior of the surface and make it more difficult to protect the substrate from corrosion. This is due to the fact that a very rough topography requires special care to insure that the peaks of the roughened surface are covered by an adequate coating thickness (109). Surface roughness has to be quantified if one wants to understand its effect on service life. Diamond stylus profilometry is one common method used for this purpose. This technique records a surface profile from which various roughness parameters such as  $R_a$  (the arithmetic average roughness) and  $R_{MAX}$  (its largest single deviation, can be calculated (110). Although these parameters are widely accepted and used, they are not sufficiently descriptive to correlate surface texture with other surface related measurements such as BET surface area or particle re-entrainment. Fractal analysis has been used to quantify roughness of various surfaces. Figure 35 shows the appearance of surfaces with different fractal numbers. In this example a computationally fast procedure based on fractal analysis techniques for remotely measuring and quantifying the perceived roughness of thermographically imaged, shot, grit and sandblasted surfaces was used (109). The computer generated surfaces compare quite favorably in roughness to the perceived roughness of actual blasted surfaces and provide a three dimensional picture correlating fractal dimension with appearance. Another approach involves application of a fractal determination method to surface profiles to yield fractal-based roughness parameters (110,111). With this technique, roughness is broken

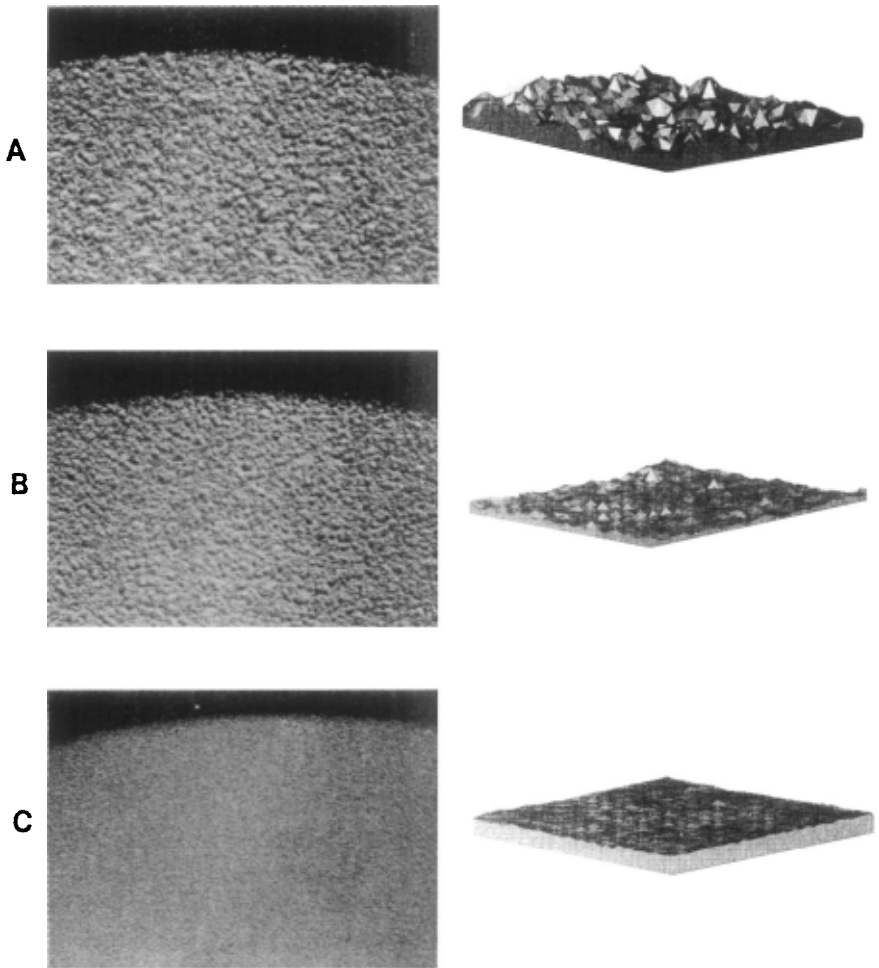


**Figure 35:** Comparison of surfaces showing blasted steel surfaces on left and computer generated surfaces on right: (A) 5 mil shot blasted surface,  $D = 2.69$ , computer  $D = 2.80$ ; (B) 2.5 mil shot blasted surface,  $D = 2.48$ , computer  $D = 2.50$ ; and (C) 0.5 mil sand blasted surface,  $D = 2.24$ , computer  $D = 2.20$ . From reference 109. Reprinted with permission of Journal of Coatings Technology.

down into size ranges rather than a single number. This provides a parameter for quantifying the finer structures of a surface. The technique involves use of a Richardson plot and is referred to as "box counting" or the "box" method (110-113). The following description on its implementation

is from Chesters et. al. (111). "This method overlays a profilometer curve with a uniform grid or a set of "boxes" of side length  $b$ , and a count is made of the non-empty boxes  $N$  shown in Figure 36, Then the box size is changed and the count is repeated. Finally, the counts are plotted against each box on a log-log scale to obtain a boxcount plot (Figure 37). The box sizes are back calculated to correspond to the physical heights they would have as features of the profile (hence, the boxcount plot shows counts versus "feature size" rather than box size). It is the absolute value of the slope which gives the fractal dimension, which is referred to as fractal based roughness ( $R_f$ ). The slope and, hence,  $R_f$  will be greater for a rough profile than for a smooth profile."

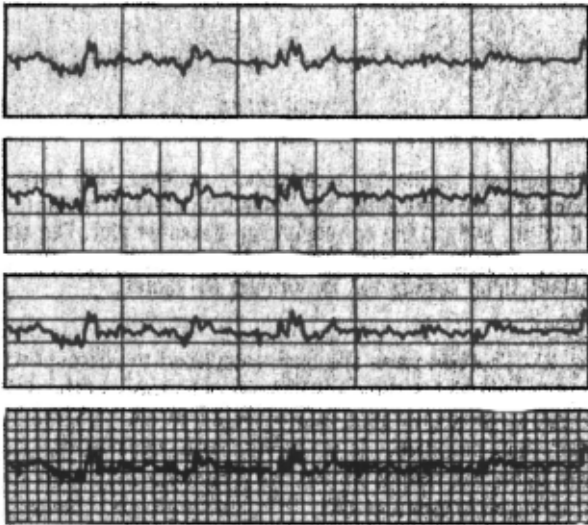


**Figure 36:** Illustration of box counting as an algorithm to obtain fractal dimension. The rate at which the number of non-empty boxes increases with shrinking box size is a direct measure of fractal roughness. From reference 111. Reprinted with permission of Solid State Technology.

Figure 37 shows box count plots for 316L stainless steel tubing which was given a variety of treatments. Figure 37a is an example of a smooth, electropolished surface. The fractal roughness for the midrange is 1.03 and there is an absence of very small and very large features. Figure 37b is for a chemically polished surface and it is noticeably different from the electropolished surface shown in Figure 37a. It has a unit slope only for features larger than 1  $\mu\text{m}$  and the roughness between 1 and 0.2  $\mu\text{m}$  has two slopes (1.46 and 1.24, respectively). Also, there is a roughness below 0.2  $\mu\text{m}$  (111). Figure 37c, which is for a non-polished surface shows a picture similar to that of Figure 37b except that the roughness between 0.5 and 1.0  $\mu\text{m}$  is higher (110). This analysis provides more information than is obtainable from surface roughness measurements alone, is not limited to profilometers, and can be extended to higher resolution surface techniques (110,111).

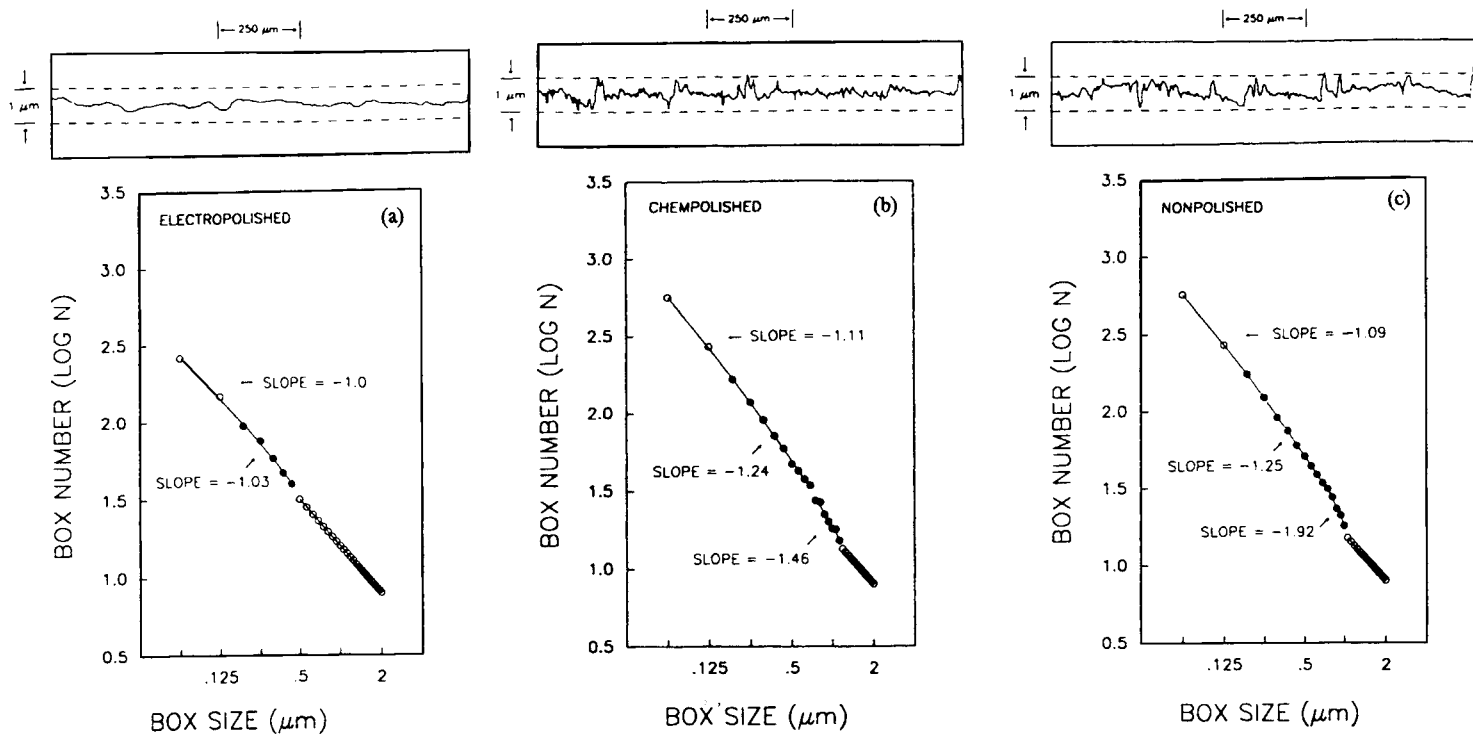


**Figure 37:** Roughness profiles and box count plots for 316 stainless steel tubing. (a) Electropolished,  $R_a = 0.05$  and  $R_{max} = 0.56$ ; (b) Chemically polished,  $R_a = 0.09$  and  $R_{max} = 1.02$ ; (c) Non-polished,  $R_a = 0.14$  and  $R_{max} = 1.06$ . From reference 110. Reprinted with permission of Elsevier Science Publishers B. V., The Netherlands.

## REFERENCES

1. R. Weil, "Structure, Brightness and Corrosion Resistance of Electrodeposits", *Plating* 61, 654 (1974).
2. N. J. A. Sloane, "The Packing of Spheres", *Scientific American*, 250, 116 (1984).
3. H. McArthur, *Corrosion Prediction and Prevention in Motor Vehicles*, Ellis Horwood Ltd., England, 166 (1988).
4. J. F. Shackelford, *Introduction to Materials Science for Engineers, Second Edition*, Macmillan Publishing Company, New York (1988).
5. C. A. Snavely, "A Theory for the Mechanism of Chromium Plating; A Theory for the Physical Characteristics of Chromium Plate", *Trans. Electrochem. Soc.*, 92, 537 (1947).
6. W. H. Safranek, *The Properties of Electrodeposited Metals and Alloys, Second Edition*, American Electroplaters and Surface Finishers Society, Orlando, FL, 1986.
7. V. A. Lamb, "Plating and Coating Methods: Electroplating, Electroforming, and Electroless Deposition", Chapter 32 in *Techniques of Materials Preparation and Handling*, Part 3, R. F. Bunshah, Editor, Interscience Publishers (1968).
8. T. G. Beat, W. K. Kelley and J. W. Dini, "Plating on Molybdenum", *Plating & Surface Finishing*, 75, 71 (Feb 1988).
9. W. Blum and G. B. Hogaboom, *Principles of Electroplating and Electroforming*, Third Edition, McGraw-Hill Book Co., (1949).
10. W. H. Safranek, "Deposit Disparities", *Plating & Surface Finishing*, 75, 10 (June 1988).
11. J. W. Dini, "Deposit Structure", *Plating & Surface Finishing*, 75, 11 (Oct 1988).
12. R. Messier and J. E. Yehoda, "Geometry of Thin-Film Morphology", *J. Appl. Phys.* 58, 3739 (1985).
13. B. A. Movchan and A. V. Demchishin, "Study of Structure and Properties of Thick Vacuum Condensates of Ni, Ti, W, Al<sub>2</sub>O<sub>3</sub> and ZrO<sub>2</sub>", *Phys. Met. Metallogr.* 28, 83 (1969).

14. J. A. Thornton, "Influence of Apparatus Geometry and Deposition Conditions on the Structure and Topography of Thick Sputtered Coatings", *J. Vac. Sci. Technol.*, 11, 666 (1974).
15. J. A. Thornton, "High Rate Thick Film Growth", *Ann. Rev. Mater. Sci.*, 7, 239 (1977).
16. J. E. Yehoda and R. Messier, "Quantitative Analysis of Thin Film Morphology Evolution", *SPIE Optical Thin Films II: New Developments*, 678, 32 (1986).
17. R. Messier, A. P. Giri and R. A. Roy, "Revised Structure Zone Model for Thin Film Physical Structure", *J. Vac. Sci. Technol.*, A2, 500 (1984).
18. J. E. Yehoda and R. Messier, "Are Thin Film Physical Structures Fractals?", *Applications of Surface Science*, 22/23, 590 (1985).
19. R. Messier, "Toward Quantification of Thin Film Morphology", *J. Vac. Sci. Technol.*, A4, 490 (May/June 1986).
20. R. Weil, *Electroplating Engineering Handbook*, Fourth Edition, L. J. Durney, Editor, Van Nostrand Reinhold, Chapter 12 (1984).
21. A. W. Hothersall, "Adhesion of Electrodeposited Nickel to Brass", *J. Electrodepositors' Tech. Soc.*, 7, 115 (1932)
22. I. Kim and R. Weil, "Tension Testing of Very Thin Electrodeposits", *Testing of Metallic and Inorganic Coatings*, ASTM STP 947, W. B. Harding and G. A. DiBari, Eds., American Society for Testing and Materials, Philadelphia, PA, pp. 11-18 (1987).
23. R. Haak, C. Ogden and D. Tench, "Comparison of the Tensile Properties of Electrodeposits From Various Acid Copper Sulfate Baths", *Plating & Surface Finishing*, 68, 59 (Oct 1981).
24. W. D. Fields, R. N. Duncan, and J. R. Zickgraf, "Electroless Nickel Plating", *Metals Handbook*, Ninth Edition, Vol 5, *Surface Cleaning, Finishing and Coating*, ASM, Metals Park, Ohio (1982).
25. H. G. Schenzel and H. Kreye, "Improved Corrosion Resistance of Electroless Nickel-Phosphorus Coating", *Plating & Surface Finishing*, 77, 50 (Oct 1980).
26. "The Engineering Properties of Electroless Nickel Deposits", INCO, New York, NY (1977).

27. D. H. Johnson, "Thermal Expansion of Electroless Nickel", *Report 28-670, Y-12 Plant*, Oak Ridge National Laboratory, Oak Ridge, TN, (Jan 2, 1982).
28. D. H. Killpatrick, "Deformation and Cracking of Electroless Nickel", *AFWL-TR-83*, Air Force Weapons Laboratory, Kirtland Air Force Base, NM (Jan 1983).
29. M. W. Mahoney and P. J. Dynes, "The Effects of Thermal History and Phosphorus Level on the Crystallization Behavior of Electroless Nickel", *Scripta Metallurgia*, 19, 539 (1985).
30. H. J. Wiesner and W. B. Distler, "Physical and Mechanical Properties of Electroformed Gold-Copper Alloys", *Plating*, 56, 799 (1969).
31. J. W. Price, "Tin and Tin-Alloy Plating", *Electrochemical Publications Limited* (1983).
32. C. F. Hornig and J. F. Bohland, "Electrodeposited Tin-Nickel Stability", *Scripta Metallurgia*, 11, 301 (1977).
33. M. R. Pinnel, "Diffusion Related Behavior of Gold in Thin Film Systems", *Gold Bulletin*, 12, No 2, 62 (April 1979).
34. C. J. Raub, Proc. Symposium on Economic Use of and Substitution for Precious Metals in the Electronics Industry, *American Electroplaters & Surface Finishers Soc.*, Danvers, Mass. (1980).
35. S. Jayakrishnan and S. R. Natarajan, "Hydrogen Codeposition in Palladium Plating", *Metal Finishing* 89, 23 (Jan 1991).
36. S. Nakahara and S. Mahajan, "The Influence of Solution pH on Microstructure of Electrodeposited Cobalt", *J. Electrochemical Soc.*, 127, 283 (1980).
37. S. Nakahara and E. C. Felder, "Defect Structure In Nickel Electrodeposits", *J. Electrochem. Soc.*, 129, 45 (1982).
38. R. S. Montgomery and F. K. Sautter, "Factors Influencing the Durability of Chrome Plate", *Wear*, 60, 141 (1980).
39. C. Conte, G. Devitofrancesco and V. DiCastro, "Study of the Behavior of Protective Metal Surfaces in the Presence of Gas by X-ray, Photoelectron Spectroscopy", *Surface and Coating Technology*, 34, 155 (1988).

40. T. Barbee, Lawrence Livermore National Laboratory, private communication, May 1989.
41. H. J. Wiesner and W. J. Frey, "Some Mechanical Properties of Copper Deposited From Pyrophosphate and Sulfate Solutions", *Plating & Surface Finishing*, 66, 51 (Feb 1979).
42. B. M. Hogan, "Microstructural Stability of Copper Electroplate" *Proceedings SUR/FIN 84*, American Electroplaters & Surface Finishers Soc., Orlando, Fl. (1984)
43. T. T. Saito, "Polishing and Characterizing Diamond Turned Optics". Lawrence Livermore Laboratory, *UCRL 51951*, Nov 3, 1975.
44. N. P. Fedotov, P. M. Vyacheslavov, and V. I. Gribel, *Journal of Applied Chemistry (USSR)*, 37 (6), 1368 (1964).
45. J. P. Celis, J. R. Roos and C. Buelens, "Texture in Metallic, Ceramic and Composite Coatings", *Directional Properties of Materials*, H. J. Bunge, Editor, DGM Informationsgesellschaft mbH, Oberursel, Germany, 189 (1988).
46. S. J. Shaffer, J. W. Morris, Jr., and H.-R. Wenk, "Textural Characterization and its Application on Zinc Electroplated Steels", *Zinc-Based Steel Coating Systems: Metallurgy and Performance*, G. Krauss and D. K. Matlock, Editors, The Minerals, Metals & Materials Society, 129 (1990).
47. C. S. Barrett, *Structure of Metals*, Second Edition, McGraw-Hill, New York (1952).
48. J. Amblard, I. Epelboin, M. Froment and G. Maurin, "Inhibition and Nickel Electrocrystallization", *Jour. of Applied Electrochemistry*, 9, 233 (1979).
49. C. M. Vlad, "Texture and Corrosion Resistance of Metallic Coatings", *Directional Properties of Metallic Coatings*, H. J. Bunge, Editor, DGM Informationsgesellschaft mbH, Oberursel, Germany, 199 (1988).
50. A. J. Perry and L. Simmen, "Ion-Plated HfN Coatings", *Thin Solid Films*, 118, 271 (1984).
51. A. J. Perry, "The Structure and Colour of Some Nitride Coatings", *Thin Solid Films*, 135, 73 (1986).

52. E. Schmid and W. Boas, *Plasticity of Crystals*, English translation published by F. A. Hughes & Co. (1950).
53. S. J. Shaffer, A. M. Philip and J. W. Morris, Jr., "Micromechanisms of Surface Friction in Zinc Electrogalvanized Steel Sheets", *Proceedings Galvatech 89 Conference*, Tokyo, Japan (Sept 1989).
54. J. H. Lindsay, R. F. Paluch, H. D. Nine, V. R. Miller and T. J. O'Keefe, "The Interaction Between Electrogalvanized Zinc Deposit Structure and the Forming Properties of Sheet Steel", *Plating & Surface Finishing*, 76, 62 (March 1989).
55. J. H. Lindsay, "Electrogalvanized Automotive Sheet Steel and the Manufacturing System", *Proceedings SUR/FIN 91, American Electroplaters and Surface Finishers Soc.*, Orlando, Fl., 25 (1991).
56. G. Krauss and D. Matlock, Editors, *Zinc-Based Steel Coating Systems: Metallurgy and Performance*, The Minerals, Metals & Materials Society (1990).
57. A. T. Gwathmey, "Effect of Crystal Orientation on Corrosion", *The Corrosion Handbook*, H. H. Uhlig, Editor, Wiley & Sons, (1948).
58. J. L. Weininger and M. W. Bretter, "Effect of Crystal Structure on the Anodic Oxidation of Nickel", *J. Electrochemical Soc.*, 110, 484 (1963).
59. G. Raichevski and T. Milusheva, "Effect of the Texture and Structure of the Surface of Electroplated Nickel on its Corrosion and Electrochemical Behavior in an Acid Medium", *Protection of Metals*, 11, No 5, 519 (Sept/Oct 1975).
60. H. Takechi, M. Matsuo, K. Kawasaki and T. Tamura, *Proceedings 6th Int. Conf. on Textures of Materials*, Vol 2, 209, (1981), Tokyo.
61. R. F. Ashton and M. T. Hepworth, "Effect of Crystal Orientation on the Anodic Polarization and Passivity of Zinc", *Corrosion*, 24, 50 (1968).
62. V. Rangarajan, N. M. Giallourakis, D. K. Matlock and G. Krauss, "The Effect of Texture and Microstructure on Deformation of Zinc Coatings", *J. Mater. Shaping Technol.*, 6, 217 (1989).

63. N. J. Nelson, P. A. Martens, J. F. Battey, H. R. Wenk and Z. Q. Zhong, "The Influence of Texture on the Etching Properties of Copper Foil", *Eighth International Conference on Textures of Materials*, J. S. Kallend and G. Gottstein, Editors, The Metallurgical Soc/AIME, Warrendale, PA., 933 (1988).
64. J. F. Battey, N. Nelson and P. A. Martens, "Etching Electrodeposited Copper Foil", *PC Fab 10*, 60 (Dec 1987).
65. I. Artaki, M. H. Papalski and A. L. Moore, "Copper Foil Characterization and Cleanliness Testing", *Plating & Surface Finishing*, 78, 64 (Jan 1991).
66. H. Leidheiser, Jr., "Coatings", *Corrosion Mechanisms*, F. Mansfeld, Editor, Marcel Dekker, Inc., 165 (1987).
67. H. Leidheiser, Jr., and D. K. Kim, "Crystallographic Factors Affecting the Adherence of Paint to Deformed Galvanized Steel", *Journal of Metals*, 28, 19 (Nov 1976).
68. T. F. Davis and D. Kahn, "Contact Resistance of Oriented Electroplated Nickel", Proceedings SUR/FIN 91, *American Electroplaters & Surface Finishers Soc.*, Orlando, FL., 329 (1991).
69. M. Schlesinger, X. Meng, W. T. Evans, D. A. Saunders and W. P. Kampert, "Micromorphology and Magnetic Studies of Electroless Cobalt/Phosphorus Thin Films", *J. Electrochem. Soc.*, 137, 1706 (1990).
70. R. J. Morrissey, "The Electrodeposition of Palladium From Chelated Complexes", *Platinum Metals Review*, 27, No. 1, 10 (1983).
71. M. Kobayashi and Y. Doi, "TiN and TiC Coating on Cemented Carbides by Ion Plating", *Thin Solid Films*, 54, 67 (1978).
72. J. A. Sue and H. H. Troue, "Effect of Crystallographic Orientation on Erosion Characteristics of Arc Evaporation Titanium Nitride Coating", *Surface and Coating Technology*, 33, 169 (1987).
73. V. Tomov, D. S. Stoychev and I. B. Vitanova, "Recovery and Recrystallization of Electrodeposited Bright Copper Coatings at Room Temperature. II. X-ray Investigation of Primary Recrystallization", *J. Applied Electrochemistry*, 15, 887 (1985).

74. F. Argoul, A. Arneodo, G. Grasseau, and H. L. Swinney, "Self-Similarity of Diffusion-Limited Aggregates and Electrodeposition Clusters", *Physical Review Letters*, 61, 2558 (1988).
75. L. M. Sander, "Fractal Growth", *Scientific American*, 256, 94 (Jan. 1987).
76. J. McDermott, "Geometrical Forms Known as Fractals Find Sense in Chaos", *Smithsonian*, 14, 110 (Dec 1983).
77. A. L. Goldberger, D. R. Rigney and B. J. West, "Chaos and Fractals In Human Physiology", *Scientific American* 262, 43 (Feb 1990).
78. A. Seri-Levy and D. Avnir, "Fractal Analysis of Surface Geometry Effects on Catalytic Reactions", *Surface Science*, 248, 258 (1991).
79. E. Hornbogen, "Fractals in Microstructure of Metals", *International Materials Reviews*, 34, No 6, 277 (1989).
80. F. F. Ling, "Fractals, Engineering Surfaces, and Tribology", *Wear*, 136, 141 (1990).
81. B. B. Mandelbrot, D. E. Passoja and A. J. Paullay, "Fractal Character of Fracture Surfaces of Metals", *Nature*, 308, 721 (April, 1984).
82. E. E. Underwood and K. Banerji, "Fractals in Fractography", *Materials Science and Engineering*, 80, 1 (1986).
83. C. S. Pande, L. R. Richards and S. Smith, "Fractal Characteristics of Fractured Surfaces", *Jour. of Materials Science Letters*, 6, 295 (1987).
84. Z. H. Huang, J. F. Tian and Z. G. Wang, "Analysis of Fractal Characteristics of Fractured Surfaces by Secondary Electron Line Scattering", *Materials Science and Engineering*, A118, 19 (1989).
85. J. J. Mecholsky, D. E. Passoja, and K. S. Feinberg-Ringel, "Quantitative Analysis of Brittle Fracture Surfaces Using Fractal Geometry", *Jour. American Ceramic Soc.*, 72, (1), 60 (1989).
86. S. Zhang and C. Lung, "Fractal Dimension and Fracture Toughness", *Jour. Phys. D: Applied Physics*, 22, 790 (1989).

87. K. Ishikawa, "Fractals in Dimple Patterns of Ductile Fracture", *Jour. Materials Science Letters*, 9, 400 (1990).
88. R. R. Dauskardt, F. Haubensak and R. O. Ritchie, "On the Interpretation of the Fractal Character of Fracture Surfaces", *Acta. Metall.* 38, 143 (1990).
89. J. R. Ding and B. X. Liu, "Fractal Corrosion of Alloy Films by Acid", *J. Phys.: Condens. Matter*, 2, 1971 (1990).
90. G. Daccord, "Chemical Dissolution of a Porous Medium by a Reactive Fluid", *Physical Review Letters*, 58, 479 (1987).
91. J. M. Costa, F. Sagues and M. Vilarrasa, "Fractal Patterns From Corrosion Pitting", *Corrosion Science*, 32, 665 (1991).
92. B. B. Mandelbrot, *The Fractal Geometry of Nature*, W. H. Freeman & Co., New York (1977).
93. H. Jurgens, H. O. Peitgen and D. Saupe, "The Language of Fractals", *Scientific American*, 262, 60 (Aug 1990).
94. B. H. Kaye, *A Random Walk Through Fractal Dimensions*, VCH Publishers, England (1989).
95. M. LaBrecque, "Fractal Symmetry", *Mosaic*, 16, 14 (Jan/Feb 1985).
96. M. LaBrecque, "Fractal Applications", *Mosaic*, 17, 34 (Winter 1986/7).
97. A. P. Pentland, "Fractal Based Description of Natural Scenes", *IEEE Trans. on Pattern Analysis and Machine Intelligence*, Vol. PAMI-6, 661 (Nov 1984).
98. T. A. Heppenheimer, "Routes to Chaos", *Mosaic*, 17, 2 (Summer 1986).
99. F. Sagues, F. Mas, M. Vilarrasa and J. M. Costa, "Fractal Electrodeposits of Zinc and Copper", *J. Electroanal. Chem.*, 278, 351 (1990).
100. R. F. Voss and M. Tomkiewicz, "Computer Simulation of Dendritic Electrodeposition", *J. Electrochem. Soc.*, 132, 371 (1985).
101. T. Hepel, "Effect of Surface Diffusion In Electrodeposition of Fractal Structures", *J. Electrochem. Soc.*, 134, 2685 (1987).

102. A. S. Paranjpe, S. Bhakay-Tamhane and M. B. Vasan, "Two Dimensional Fractal Growth by Diffusion Limited Aggregation of Copper", *Physics Letters A*, 140, 193 (Sept. 18, 1989).
103. C.-Peng Chen and J. Jorne, "Fractal Analysis of Zinc Electrodeposition", *J. Electrochem. Soc.*, 137, 2047 (1990).
104. G. L. M. K. S. Kahanda and M. Tomkiewicz, "Fractality and Impedance of Electrochemically Grown Silver Deposits", *J. Electrochem. Soc.*, 137, 3423 (1990).
105. L. Nyikos and T. Pajkossy, "Electrochemistry at Fractal Interfaces: The Coupling of ac and dc Behavior at Irregular Electrodes", *Electrochimica Acta*, 35, 1567 (1990).
106. J. M. Gomez-Rodriguez and A. M. Baro, "Fractal Characterization of Gold Deposits by Scanning Tunneling Microscopy", *J. Vac. Sci. Technol.*, B9, 495 (Mar/Apr 1991).
107. V. Fleury, "On A New Example of Ramified Electrodeposits", *J. Mater. Res.* 6, 1169 (1991).
108. T. A. Witten, Jr., and L. M. Sander, "Diffusion-Limited Aggregation, a Kinetic Critical Phenomenon", *Physical Review Letters*, 47, 1400 (Nov. 9, 1981).
109. J. W. Martin and D. P. Bentz, "Fractal-Based Description of the Roughness of Blasted Steel Panels", *Journal of Coatings Technology*, 59, No 745, 35 (Feb 1987).
110. S. Chesters, H. Y. Wen, M. Lundin and G. Kaspar, "Fractal-Based Characterization of Surface Texture", *Applied Surface Science*, 40, 185 (1989).
111. S. Chesters, H-C. Wang and G. Kasper, "A Fractal-Based Method for Describing Surface Texture", *Solid State Technology*, 34, 73 (Jan 1991).
112. L. F. Richardson, *General Systems Yearbook*, 6, 139 (1961).
113. B. B. Mandelbrot, "Fractals in Physics", *Proc. Sixth Trieste International Symposium*, L. Pietronero and E. Tosatti, Editors, Elsevier, New York, 10 (1986).